CHALMERS
UNIVERSITY OF TECHNOLOGY

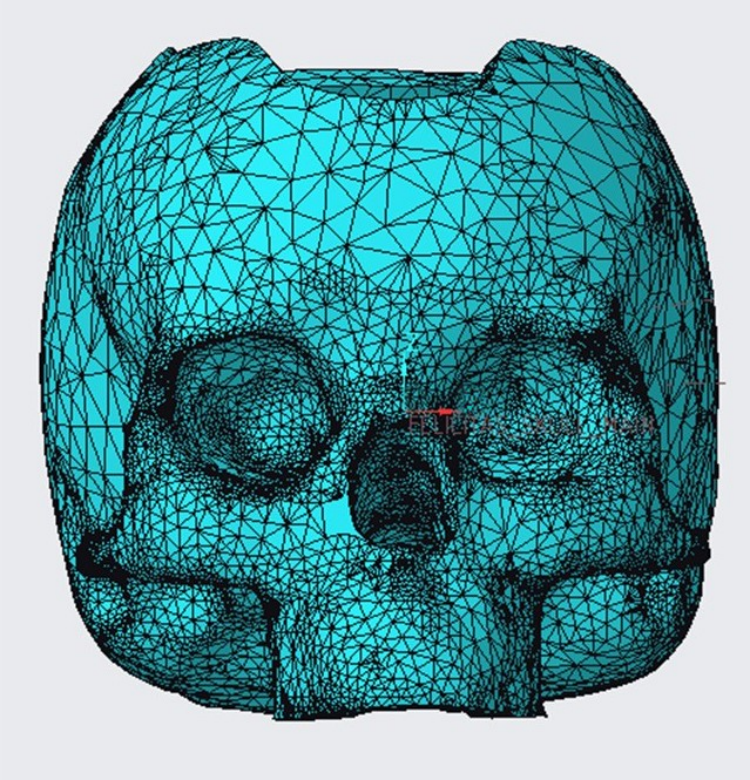

Development and evaluation of binaural and transcranial bone conduction stimulation on anatomic head simulator

In cooperation with Cochlear Bone Anchored Solutions AB

Laura Lindel

DEPARTMENT OF SOME SUBJECT OR TECHNOLOGY

CHALMERS UNIVERSITY OF TECHNOLOGY
Gothenburg, Sweden 2025
www.chalmers.se

Master's thesis 2025

Development and evaluation of binaural and transcranial bone conduction stimulation on anatomic head simulator

Laura Lindel

CHALMERS
UNIVERSITY OF TECHNOLOGY

Department of Architecture and Civil Engineering
Division of Applied Acoustics
Chalmers University of Technology
Gothenburg, Sweden 2025

Development and evaluation of binaural and transcranial bone conduction stimulation on anatomic head simulator
Laura Lindel

Supervisor: Jona Hoffmann, Cochlear Bone Anchonred Solutions AB
Examiner: Jens Ahrens, Architechture and Civil Engineering

Master's Thesis 2025
Department of Architecture and Civil Engineering
Division of Applied Acoustics
Chalmers University of Technology
SE-412 96 Gothenburg
Telephone +46 31 772 1000

Cover: Visualization of anatomic head simulator

Typeset in LaTeX
Printed by Chalmers Reproservice
Gothenburg, Sweden 2025

Development and evaluation of binaural and transcranial conduction stimulation on anatomic head simulator
Laura Lindel
Department of Architecture and Civil Engineering
Chalmers University of Technology

Abstract

Previous research has demonstrated that patients with bone conduction hearing loss can benefit from binaural fitting using bone conduction hearing devices [1]. However, certain limitations persist due to the complex vibrational patterns that arise from multiple transmission pathways within the complex skull. Notably, transcranial attenuation (TA) below 1 kHz has been reported to be approximately 0 dB SPL, with higher attenuation towards higher frequencies, allowing sound energy to propagate across the skull and stimulate both cochleae simultaneously [2].

To investigate a more realistic perception of different sound scenarios with bone conduction hearing aids, a specialized head simulator was developed by Cochlear Bone Anchored Solutions AB, modeled after a human skull and equipped with three-dimensional accelerometers positioned at the cochlear locations. This Master's thesis aimed to enable real-time audio playback from bone conduction hearing aids and simulate binaural fittings. To achieve this, digital signal processing was applied, a vector projection of the axis onto the excitation force was performed, and filters were designed to align the output with the air conduction threshold. Finally, a listening experiment involving 37 normal-hearing participants was conducted to evaluate the simulator's performance. Speech reception thresholds (SRTs) in noise were measured using the standardized Swedish Matrix (Hagerman) test, and binaural intelligibility level differences (BILD) were calculated to assess participants' ability to utilize spatial cues during headphone-based listening. Four test conditions were evaluated, involving co-located sources as well as configurations with speech presented from the front and noise positions at 270° azimuth. Measurements were conducted with both one and two BAHIs attached.

Initial measurements confirmed that transcranial attenuation (TA) values are consistent with literature findings, showing minimal attenuation below 1 kHz and increasing at higher frequencies. The resulting speech reception threshold (SRT) scores revealed a systematic shift of approximately 3 dB toward better signal-to-noise ratios (SNRs) compared to previous studies. An ILD and BILD of approximately 3.6 dB SPL confirmed the simulator's ability to reliably replicate binaural hearing.

Keywords: bone conduction, binaural fitting, transcranial attenuation, Head Simulator, Digital Signal Processing, Speech Reception Threshold, BILD,

Acknowledgements

First, I would like to express my deepest gratitude to my supervisor, Jona Hoffmann, for patiently guiding me throughout this Master's thesis. Thank you for always making time for me, for explaining the unfamiliar topics, and for answering my questions. I am truly grateful for the opportunity to collaborate with Cochlear Bone Anchored. Solutions AB, and to explore so many exciting new areas. Being part of the team has been a wonderful experience, and I will genuinely miss working with you.

I would also like to thank my professor, Jens Ahrens, for your constant support and invaluable advice. You always helped me navigate complex topics with greater confidence and understanding.

To my family, especially my mother, thank you for standing by me during the moments of doubt and overwhelm. You kept me grounded, reminded me of my strength, and believed in me even when I struggled to believe in myself. Thank you for guiding me through every storm and accompanying me while I am chasing my dreams.

A huge thank you goes to all of my friends, who were my anchors during the most stressful times. Your presence, encouragement, and all the wonderful moments we shared gave me so much strength and made Sweden feel like my second home.

Laura Lindel, Gothenburg, October 2025

List of Acronyms

Below is the list of acronyms that have been used throughout this thesis, listed in alphabetical order:

AC	Air conduction
BC	Bone conduction
BAHI	Bone Conduction Hearing Implant
BILD	Binaural Intelligibility Level Difference
CROS	Contralateral Routing of Signal
CPSD	Cross-Power Spectral Density
DSP	Digital Signal Processing
FFT	Fast Fourier Transform
FRF	Frequency Response Function
IIR	Infinite Impulse Response
ILD	Interaural Level Difference
ILD	Intelligibility Level Difference
ITD	Interaural Time Difference
LDV	Laser Doppler Vibrometry
LTI	Linear time-invariant
RMS	Root Mean Square
RSS	Root-Sum-of-Squares
SD	Standard Deviation
SNR	Signal to Noise Ratio
SRT	Speech Recognition Threshold
TA	Transcranial Attenuation
FIR	Finite Impulse Response

Nomenclature

Below is the nomenclature of indices, sets, parameters, and variables that have been used throughout this thesis.

Indices

AC	Index for air conduction
BC	Index for bone conduction
R	Index for right side
L	Index for left side
$Sens$	Index for sensitivity
i, j	Indices for distribution network buses
t	Index for time step
X	Index for spatial position or test condition (e.g., azimuthal angle or loudspeaker location)
f	Index for frequency
x, y, z	Cartesian axes for triaxial acceleration and force measurements

n Discrete-time sample index

Sets

$\mathcal{F}$	Set of frequency bins used in spectral analysis
$\mathcal{X}$	Set of spatial positions or test conditions (e.g., loudspeaker locations)

Parameters

$\mathrm{HS}_{\mathrm{Sens}}$	Head simulator sensitivity [V/N]

$\mathrm{HL_{BC}}$	Minimal hearing level for bone conduction [dBre1N]
$\mathrm{HP_{Sens}}$	Sensitivity of Sennheiser HD650 headphones [dBSPL/1Vrms]
$\mathrm{HL_{AC}}$	Minimal audible sound pressure level for air conduction [dBSPL]

Variables

$X[n]$	Original sampled discrete-time signal
$Y[n]$	Windowed signal
$W[n]$	Window function (e.g., Hanning window)
$X(f_n)$	Fourier transform of input signal at frequency bin f_n
$Y(f_n)$	Fourier transform of output signal at frequency bin f_n
$X^*(f_n)$	Complex conjugate of $X(f_n)$
N_{avg}	Number of averages in spectral estimation
$G_{xx}(f_n)$	Auto-power spectral density of input signal at frequency f_n
$G_{yx}(f_n)$	Cross-power spectral density between output and input at f_n
$H(f_n)$	Frequency Response Function (FRF) at frequency f_n
$\lvert A\rvert$	Magnitude of acceleration vector
$\mathrm{Acc}_{(xyz)}$	Triaxial acceleration data
A_{xyz}	Complex acceleration frequency function
A_x, A_y, A_z	Acceleration amplitudes in the x-, y-, and z-directions
RSS	Root-Sum-of-Squares of triaxial acceleration amplitudes
$\mathrm{ILD}_{(X)}$	Intelligibility Level Difference at position X
SRT_{S0N0}	Speech Recognition Threshold with speech and noise from the front
$\mathrm{SRT}_{S0N,x}$	SRT with speech from front and noise from position x
BILD_X	Binaural Intelligibility Level Difference at position X
$\mathrm{SRT}_{\mathrm{monaural},X}$	Monaural Speech Recognition Threshold at position X
$\mathrm{SRT}_{\mathrm{binaural},X}$	Binaural Speech Recognition Threshold at position X
H_{xyz}	Frequency Response Function from triaxial acceleration and force
F	Complex force sensor frequency function
$H(fn)$	Frequency Response Function at frequency f
$G_{yx}(fn)$	Cross-power spectral density between input $x(t)$ and output $y(t)$
$G_{xx}(fn)$	Auto-power spectral density of input signal $x(t)$
α	Angle between vector and projection axis
θ	Angle between axis and its corresponding normal plane
$\mathrm{Vector\ comp.}_{(xyz)}$	Projected acceleration component along axis (xyz)

a_0	Filter coefficient applied to the direct (non-delayed) path
a_1	Filter coefficient applied to the one-sample delayed path
z^{-1}	One-sample delay operator in discrete-time filter systems

Contents

List of Figures

List of Tables

1
Introduction

By the year 2050, an estimated 2.5 billion people worldwide will experience "some degree of hearing loss. Such impairment can significantly affect an individual's quality of life and overall well-being in many ways. Causes for hearing impairments can be, among other things, age-related, due to genetic predisposition, sickness, or environmental impacts such as loud noise exposure [3]. When left untreated, it can lead to a cognitive decline and is associated with a higher risk of suffering from dementia [4]. Moreover, hearing impairments may contribute to social isolation and the development of depressive symptoms [5]. Those are just a few examples emphasizing the need for medical devices to compensate for the different types and degrees of hearing loss.
Cochlear® is recognized as one of the global leaders in implantable hearing solutions. The Australian-based company offers a wide range of technologies, including cochlear implants, bone conduction hearing systems such as the Osia® and the Baha® System designed to address different types of hearing impairments [6].

1.1 Background

A bone-anchored hearing implant (BAHI) is a specialized solution for individuals with conductive or mixed hearing loss, as well as those experiencing single-sided deafness. It is particularly beneficial for patients with a non-functional middle ear, where traditional air conduction hearing aids are ineffective, since sound transmission to the inner ear is hindered. For this type of fitting, a bone conduction implant is fixed to the mastoid, providing a mounting point for the sound Processor, which converts sound signals into vibrational signals [7]. During the development of a new bone-anchored hearing system, numerous tests are performed on an anatomical head simulator. At Cochlear Bone Anchored Solutions AB, a new anatomical head simulator is currently under development to more accurately replicate real-world scenarios, including binaural fittings and configurations for single-sided deafness. The current head simulator is shaped like a sphere filled with a surrogate brain material and contains several one-dimensional accelerometers for measurements. Meanwhile, the new head simulator is a 3D printed skull based on a few magnetic resonance images (MRIs). It is filled with perma-gel imitating the brain mass. The optimal material for the brain mass was chosen based on a previous Master's thesis [8]. Since studies have revealed that the vibrational motion within the cochlea is Three-dimensional, an accelerometer with three axes has been integrated in the cochlear regions [9]. This enables the investigation of complex wave propagation from one side (ipsilateral) to the opposite side (contralateral), as well as the execution of binaural measurements that more closely match real-world data. Vibrations reaching the opposite ear primarily propagate through the skull bone, soft tissues, and cerebrospinal fluid. The energy loss during this propagation, also called transcranial attenuation (TA), depends on the loca-

tion of the excitation force, bone structure, and frequency [10]. Since the accelerometer in the new head simulator captures the motion in three different directions perpendicular to each other, the question arises how these three channels should be combined to mimic the human cochlear response to vibrational stimuli. In a previous Master's thesis, where a similar head simulator was utilized, the following approach was chosen: The head simulator was a 3D-printed model based on the MRI scan of a Cochlear® employee. Firstly, the subject's bone conduction (BC) hearing threshold was measured at four distinct stimulation positions. Additionally, the air conduction (AC) threshold was recorded. Using these results, a model was built that combines both pathways to compute the corresponding impulse response. However, this approach resulted in a metallic sound quality, which likely indicates the presence of signal distortion and auditory artifacts [11]. Additionally, this approach was specific to the replica of the employee; how other head simulators could be treated is still unclear.

1.2 Aim

This Master's thesis aims to advance the development of the head simulator and evaluate the binaural bone conduction stimulation for future product testing and listening experiments.

1.3 Objectives

To achieve the goal, the following steps will be undertaken.

- This study evaluates the transcranial transmission characteristics of the newly developed a head simulator, with results being compared to existing literature.
- The three-dimensional accelerometer data shall be treated to create an effective vibration response. The method of vector projection shall be explored, and the components will then be combined to form a single resultant vector representing the effective vibration response.
- The output signals from two accelerometers will be processed and converted into an audio signal suitable for headphone playback, aiming for a realistic listening experiment.
- A listening experiment, where the speech reception threshold (SRT) of participants is measured via headphones, will be carried out to verify the operational accuracy and reliability of the head simulator.

1.4 Demarcation

This study adopts an approach that was previously implemented in the earlier version of the head simulator, in which the vibrational output is calibrated to match the auditory threshold of an individual when listening via headphones. Alternative calibration methods or fitting strategies are not explored, as the current approach is seen as sufficient and has been validated by the inventors.
Regarding sound quality, the evaluation is based on the investigator's rating and the assessment of the supervisor, whose prior involvement in the development of the previous

head simulator provides relevant expertise. Since the goal of this study is to simulate binaural fitting functionality, this level of evaluation is considered sufficient.
The hardware used in this study was repurposed from the previously mentioned Master's thesis, which implemented a way to combine the three axes of the accelerometer. No alternative configurations were further investigated, as the existing setup performed well enough.

2

Theory

Sound emitted from a source makes particles in the air oscillate, which creates pressure fluctuations in the air, known as sound waves. When these sound waves reach the human outer ear, they are funneled through the ear canal and strike the tympanic membrane (eardrum). Vibrations are transformed into mechanical energy and transmitted to the cochlea via the ossicles (malleus, incus, and stapes) to the cochlea. The ossicles, together with the tympanic membrane, act as an enhancer of the vibrational energy to compensate for the energy loss caused by the transition from the low-impedance of air to the high-impedance of fluid within the cochlea's scala tympani, scala media, and scala vestibuli. The stapes footplate transmits the vibration through the oval window into the cochlea. Since the cochlea is filled with incompressible fluid, pressure changes are equalized through the round window, which flexes outward. Pressure changes within the scala media generate both longitudinal sound waves and surface waves, which in turn induce a passive traveling wave along the basilar membrane. [12]. According to the place theory, the traveling wave reaches its highest deflection at the basilar membrane's (BM) resonant frequency [13]. High-frequency sounds are processed at the base of the cochlea, where the basilar membrane is narrower and stiffer. In contrast, low-frequency sounds are detected at the apex, where the basilar membrane is wider, more flexible, and has a greater mass [14]. For sound pressure levels below 40 dB (SPL), the deflection of the basilar membrane is actively amplified to provide a high frequency resolution. Pressure fluctuation within the scala media causes deflection of stereocilia on top of the inner hair cells located in the organ of Corti, leading to depolarization and the generation of action potentials. From the auditory nerve, the electrical signal is transmitted to the auditory cortex. The various stages of this complex signal processing will be explored in greater detail in the chapter on the auditory pathway [15].

2.1 Bone-conduction

The previous section outlined the mechanism of air-conduction hearing, whereas bone-conduction involves more complex sound propagation through the human skull, engaging multiple different pathways. These pathways include facial bones, ossicles, and other cranial structures, which contribute to even more complicated wave patterns, leading to constructive and destructive interferences [16]. Since it is stated that the excitation from air-conduction leads to similar sound perception as through bone-conduction, the question of how vibrations are being processed within the cochlea itself arises [17]. According to R. Dauman, the vibration propagating from the transducer on the mastoid to the inner ear can be divided into two pathways. One reaches the ipsilateral cochlea directly, and one that goes via the outer, middle ear, and middle ear ossicles. The inner ear fluid inertia and pressure difference inside the cochlea is stated to be one of the main mechanisms for

auditory perception apart from the "compression of the cochlear walls" [18]. "Regardless of how vibrational energy reaches the inner ear, it ultimately stimulates the cochlea and contributes to the perception of sound" [19]. Since the transmission of vibrations through the skull and their perception is a broad subject with numerous studies and diverse findings, this thesis will focus primarily on the fundamental principles to establish a solid foundation without exceeding its intended scope. A previous Master's thesis addressed this topic in more detail, comparing various methods and outcomes, and provided a comprehensive overview. [20].

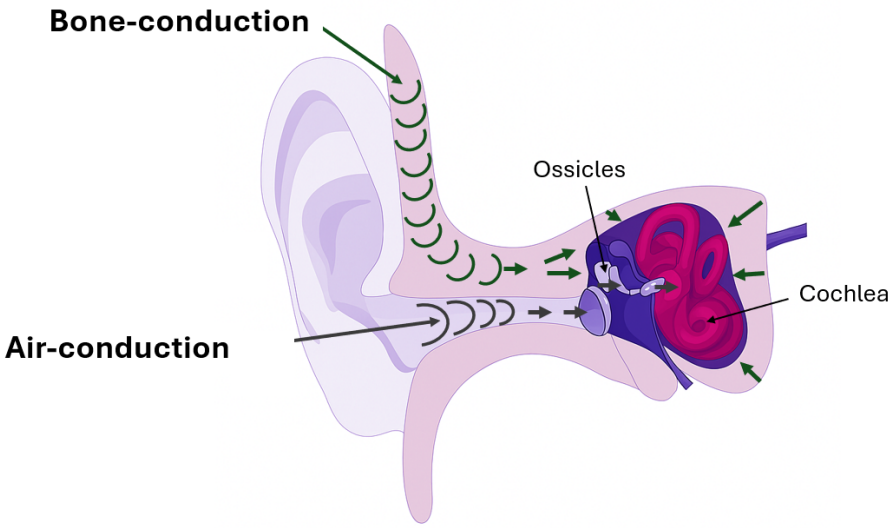

Figure 2.1: Cross-sectional illustration of auditory pathways for air conduction (AC) and bone conduction (BC) [16]. Image AI-generated with Microsoft Copilot and post-processed in PowerPoint,

2.1.1 Transcranial attenuation

Vibrations excited at one side of the head (ipsilateral) and reaching the opposite ear (contralateral) primarily propagate through the skull bone, soft tissues, and cerebrospinal fluid. The energy loss during this propagation, also called transcranial attenuation (TA), was found to range from -5 dB to 10 dB, depending on the location of the excitation force, bone structure, and frequency [10] as one can see in Figure 3.2. Below 1 kHz, the skull moves as a rigid body oscillating back and forth, and the energy loss ranges from -5 to 5 dB. Above 1 kHz, the motion transitions to transverse traveling waves, causing local deformations in the bone structure and a higher attenuation up to 10 dB [21].
Understanding the complex behavior of the human skull during stimulation with a bone-conduction hearing aid is crucial, since requirements for the different BAHI fittings can vary. In single-sided deafness fittings, where an implant is placed on the impaired side to compensate for hearing loss, low transcranial attenuation is beneficial, allowing vibrational energy to effectively reach the contralateral cochlea. In contrast, for binaural fittings, higher interaural attenuation is preferable to minimize cross-talk. Another key factor in bone-conduction hearing is the location of the excitation force. The smaller the distance, for example between transducer and cochlea, the better the sound transmission to the inner ear (ipsilateral), and the higher the sound attenuation contralaterally

[10],[22]. However, based on practical experience, differences beyond a few centimeters appear negligible. As shown in Figure 2.2, the Transcranial Attenuation (TA) remains close to 0 dB below 1 kHz, while attenuation increases progressively at higher frequencies. It is important to note that this represents a general trend, as individual variability is strongly influenced by differences in bone structure, skin thickness, and location of the excitation force [23]

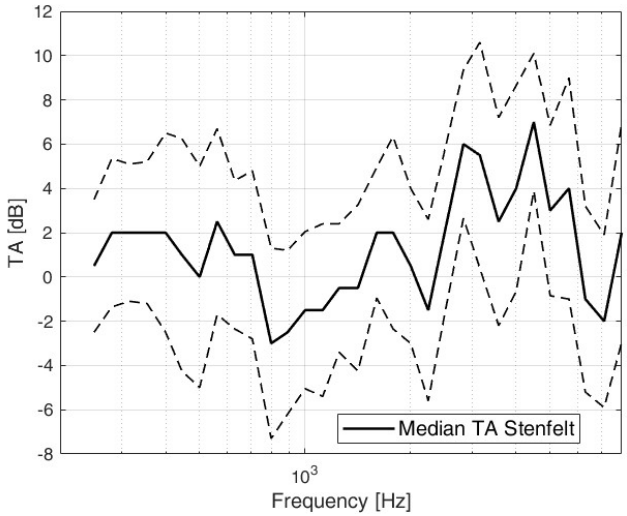

Figure 2.2: Graph of the transcranial attenuation measured in 28 participants with unilateral deafness in a study conducted by Stenfelt. The continuous line represents the median at the bone-anchored hearing implant (BAHI) position, and the dashed line (–) indicates the standard deviation (SD) across the participants [2].

2.1.2 Single-sided deafness fitting

In case of unilateral deafness, a bone-conduction hearing aid can be applied to restore auditory perception. The device captures sound from the side affected by inner ear deafness, converts it into vibrations, and transmits them through the skull to the contralateral, functioning cochlea. This process compensates for the acoustic head shadow effect, which can otherwise prevent patients from following conversations occurring on their deaf side. [24]. However, treatment with this kind of CROS device (Contralateral Routing of Signal device) does not fully restore the ability to localize sound. Since only one cochlea is functional, crucial binaural cues, such as interaural level and time differences, are absent, making it impossible for the auditory system to accurately process spatial information [25]. In complex sound environments, the greatest benefit is observed when the speech signal is presented from the side of the bone-anchored hearing implant (BAHI) or from the front, while the noise originates from the opposite side. In contrast, the reverse scenario, where noise comes from the BAHI side and the signal from the well-functioning side, can significantly reduce the signal-to-noise ratio and impair speech understanding [1].

2.1.3 Binaural fitting

Binaural hearing is based on the principle that a sound reaching both ears will exhibit differences in level, timing, phase, and spectral components. The auditory system analy-

ses these subtle variations to extract spatial cues, allowing humans to accurately localize the source of a sound, especially when the signal comes from the side [1],[26]. This is crucial for capturing and interpreting the complex sound scenery that one is being exposed to daily. It helps to separate meaningful content, such as speech, from the noisy background when sitting in a busy restaurant, for instance. Individuals with an untreated hearing impairment lack those cues, leading to worse speech discrimination in noisy environments. Focusing on a speaker helps with understanding speech in general but requires accurate sound localization and the ability to organize complex auditory environments. That's why addressing hearing loss with a well-fitted hearing aid is not just beneficial but essential, leading to a better quality of life in general [27],[28],[29].

Even if the advantages of binaural hearing are undeniable, binaural fitting with two bone-conduction hearing aids have their limitations compared to air-conductive hearing aids. One of the biggest challenges is the so-called interaural cross-talk, where vibrations transmitted through the skull can stimulate both cochleae simultaneously, as one can see in Figure 2.3. When excitation forces are applied to both sides, the resulting interaction between the signals can influence the overall stimulation pattern and consequently the auditory perception [30],[1].

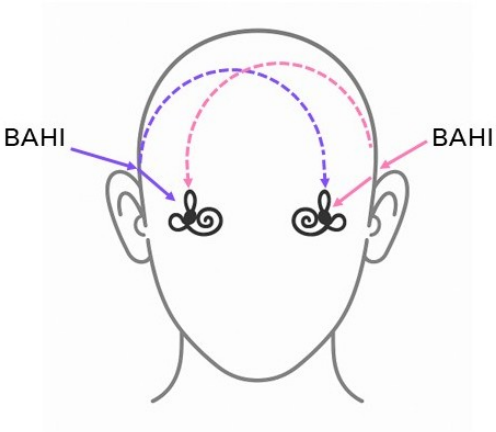

Figure 2.3: Front-view sketch of a human head illustrating crosstalk when stimulated via two bone-anchored hearing aids (BAHIs). Image AI-generated with Microsoft Copilot and post-processed in PowerPoint.

However, binaural processing in patients using bone-anchored hearing implants (BAHIs) is considered possible due to the precedence effect, which describes the auditory system's tendency to localize sounds based on the first-arriving wavefront. Additionally, a transcranial delay of approximately 0.2 ms for frequencies above 800 Hz, as vibrations travel from one cochlea to the opposite side, provides sufficient interaural time cues to support sound localization. This phenomenon can, in turn, enhance speech understanding in noisy environments [1]. While some studies have demonstrated that patients using bone-conduction hearing aids can benefit from binaural cues, it is still controversial, whether the potential advantages outweigh the surgical risks and increased expenses associated with implanting a second device. Moreover, the lack of high-quality research makes it difficult to draw definitive conclusions regarding the advantages of bilateral implantation [31] [1]. As a result, a majority of patients with symmetrical conductive hearing loss are fitted with only one bone conduction hearing aid [32].

2.1.4 Auditory pathway

Given the complexity of the auditory system, with its numerous stages and overlapping pathways, this thesis will focus only on the stages most relevant to the topic of the Master's thesis. Beginning with the generation of electrical signals by the stimulated inner hair cells, the signal is transmitted via the cochlear branch of vestibulo cochlear nerve (cranial nerve VIII) and reaches then the cochlear nuclei, where the spectral and temporal characteristics of the sound are analyzed and processed. From there, information is sent to the superior olivary complex on both the ipsilateral and contralateral sides, where interaural time and level differences (ITD, ILD) are compared. This binaural processing enables sound localization. The signal then passes through several additional processing stages, such as lateral lemniscus, inferior colliculus and medial geniculate body, before reaching the auditory cortex. There, the spatial and auditory information is integrated and interpreted, enabling recognition and understanding of speech as well as the precise localization of sound sources [33],[34]. The block diagram in Figure 2.4 illustrates that, during air-conduction stimulation, each cochlea is activated individually. In contrast, bone-conduction results in cross-talk between the cochleae, which can impair binaural processing [1].

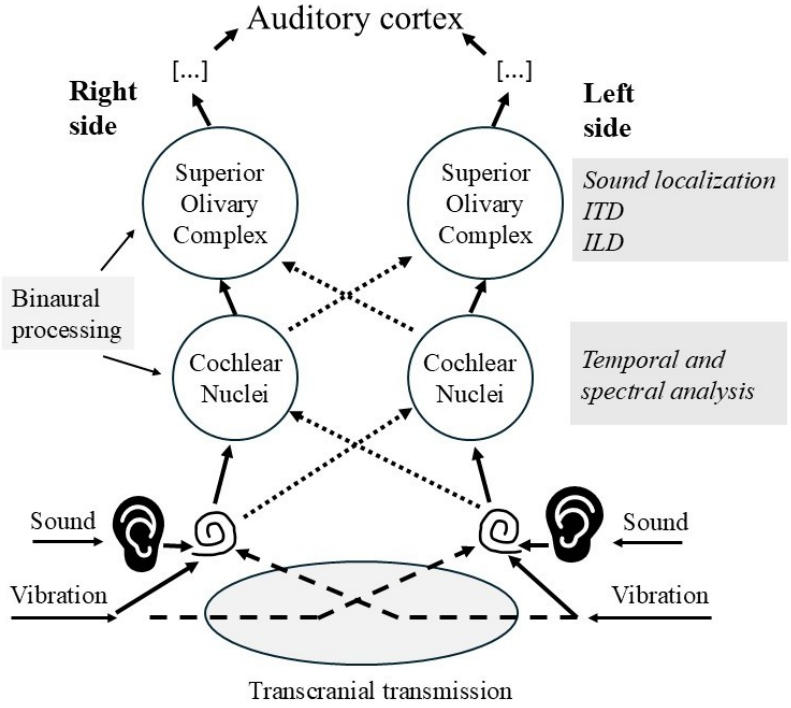

Figure 2.4: Block diagram of the auditory pathway for air and bone conduction. Vibrations are reaching the cochlea on the side of excitation as well as the opposite side with some degree of attenuation (transcranial attenuation). This phenomenon, known as cross-talk, hinders binaural processing in bone conduction hearing. In contrast, during air conduction stimulation, sound reaches each cochlea separately through the ear canal, allowing the auditory system to properly analyze and compare the temporal and spectral components as well as the interaural time differences (ITD) and the interaural level differences (ILD) for proper sound localization [1].

2.1.5 Three-dimensional response of the cochlea

A great amount of research has been done in the past in order to understand how the cochlear nerve actually responds to bone-conducted stimuli. One of the pioneer investigator was the nobel price winner Georg von Békésy with his "theory of paradoxical wave propagation", which claims that independently of the type of excitation (AC or BC) and excitation direction, the transversal wave propagates from the base to the apex of the cochlear [35],[36]. Namekeun Kim et al. designed a finite element model which simulates the behavior of the basilar membrane as well as the oval and round window. When excited by rigid body vibrations, the response of the cochlear nerve seems to be similar to air-conducted sound and independent of the direction of the excitation force and therefore supports Békésy's hypothesis.[37]. It is also of interest whether the cochlea responds equally to vibrations from different directions. A study specifically addressing this question measured hearing thresholds in live guinea pigs by recording compound action potentials following bone-conduction stimulation from five distinct directions. Simultaneously, Laser Doppler Vibrometry (LDV) was used to measure the vibration of the cochlear promontory. This approach allowed researchers to determine whether vibrations from each direction resulted in a hearing sensation, based on the correlation between cochlear motion and neural response. The study showed that vibrations along the y-axis (from right to left motion) were the primary contributors to hearing perception at frequencies below 8 kHz, while x-axis vibrations (front to back) became increasingly influential above 16 kHz. In contrast, z-axis vibrations were found to have the least impact on auditory sensation across the tested frequency range. The authors note that, in some cases, representing auditory perception using motion in a single direction may be sufficient; However, incorporating all three dimensions—each weighted differently based on the measurement data—yields the most accurate prediction of actual hearing thresholds [38].

2.1.6 Dobrev method

Based on vibration measurements in human cadaver heads with a bone-conduction hearing aid attached to the mastoid, Dobrev et al. developed a method to provide insight into the potential motion within the cochlea and interaural sound transmission. In their study, a Laser Doppler Vibrometer (LDV) was used to capture the 3D point motion of the promontory, which is the bone covering the basal turn of the cochlear nerve close to the round window. When combining the three axes, the individual phase delays were taken into account to obtain the resultant "maximum velocity vector" [39]. Since Dobrev et al.'s framework was formulated in terms of velocity, the corresponding equations were adapted to enable computation from acceleration data. This reformulation allowed for direct implementation in MATLAB and the analysis of triaxial accelerometer signals while preserving the temporal and spatial information [40].

2.2 Head simulator

Figure 2.5 shows the head simulator from both the front and the side views, along with the corresponding accelerometer coordinate system. The structure of the head simulator is predominantly continuous, with strategically placed porous regions that replicate the pneumatic chambers found in a real human skull. Accelerometers of the Dytran model

3293A [41] are affixed directly to the structure, ensuring a rigid connection at the cochlea location, which ensures direct vibration transmission.

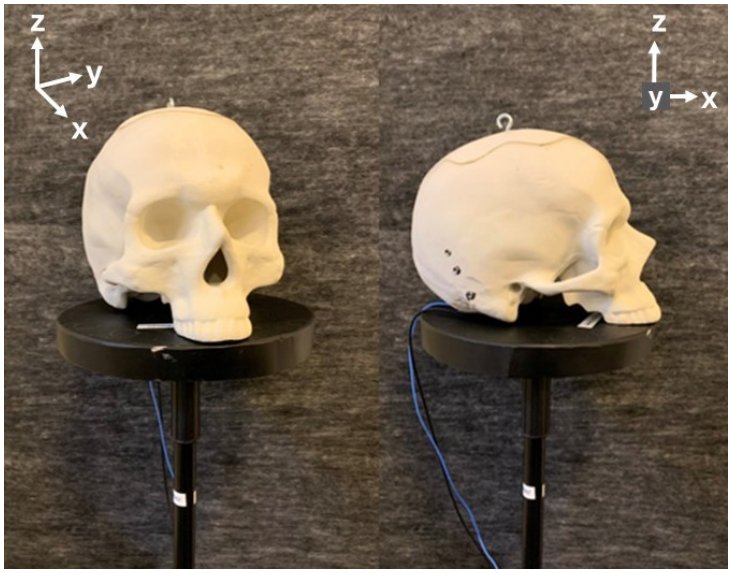

Figure 2.5: A front and side view of the head simulator Generic. The side view reveals the three screws to which the actuator of the bone-anchored hearing implant can be attached.

2.2.1 Three-dimensional accelerometer

Since it is known that a three-dimensional representation of the cochlear vibration is more realistic, the question arises of how the three axes (x,y,z) of the accelerometer be combined to result in a single vector. One way is to calculate the Root-Sum-of-Squares (RSS) as in Formula 2.1, where A represents the acceleration amplitude in the x-, y-, and z-directions, respectively. This value represents the total vibrational energy at the cochlear promontory and is less affected by constructive or destructive interference patterns [38].

$$\text{RSS} = \sqrt{A_x^2 + A_y^2 + A_z^2} \tag{2.1}$$

where:

- RSS = the Root Sum of Squares
- A = the acceleration amplitude

Another and more advanced way is through complex calculations where the phase information is being considered, leading to a maximum velocity vector as done by Dobrev et al. [39]. Since the goal of this Master's thesis is to enable real-time listening to the output of a bone-conduction hearing aid, a simplified approach is adopted. This is because the software used, SigmaStudio, is optimized for real-time audio processing and is not designed to handle complex matrix operations or phase tracking, as required by the method proposed by Dobrev. However, the Dobrev approach is still taken into account for further spectral analysis to compare the output after digital signal processing with the optimal theoretical resulting maximum vector.

2.3 Speech Reception Threshold

A common way in clinical audiology to evaluate the speech intelligibility of a patient in a noisy environment is by measuring the speech reception threshold (SRT) in free field with the signal in front and the noise source varying systematically in its location. The noise level remains constant, while the speech intensity is adaptively adjusted until the patient correctly identifies 50% of the words presented. The Signal-to-Noise Ratio (SNR) of this threshold is used for further calculations. By running the test under different conditions, such as with a single bone-anchored hearing implant (BAHI) versus bilateral BAHIs, clinicians can gain insight into the possible benefits of a binaural fitting. This can be done by comparing the different Signal-to-Noise Ratios (SNRs) of the different test settings and conditions. In addition to varying the BAHI setup, noise can be introduced from multiple azimuth angles (e.g., 0°, 90°, 270°), while the signal source remains constant, as illustrated in the Figure 2.6.

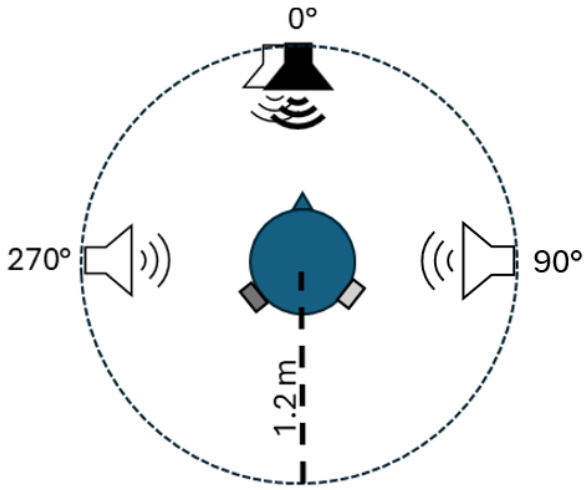

Figure 2.6: Setup for Speech Reception Threshold measurement in free field with the patient in the middle of the loudspeaker array.

The Intelligibility Level Difference (ILD) defined in equation 2.2 quantifies the improvement in speech understanding due to spatial separation between the speech and noise sources. Specifically, it reflects the difference in SNR between a co-located condition (speech and noise both from 0° azimuth, denoted as S0N0) and a spatially separated condition (speech from the front, S0, and noise from another location, Nx) [42] [43].

$$\mathrm{ILD}_{(X)} = SRT_{S0N0} - \mathrm{SRT}_{S0N}, x \quad [\mathrm{dB}] \tag{2.2}$$

where:

- ILD(X) = Intelligibility Level Difference at position X
- $\mathrm{SRT}_{\mathrm{S0N0}}$ = Signal-to-noise ratio of Speech Reception Threshold with both speech and noise from the front (reference condition)

The Binaural Intelligibility Level Difference (BILD) measures the enhancement in speech comprehension in noisy environments when using binaural hearing aids compared to monaural ones. Similarly, the Intelligibility Level Difference (ILD) reflects spatial hearing advantages under comparable conditions. A positive signal-to-noise ratio (SNR) indicates

improved intelligibility when the noise source is positioned laterally, allowing the auditory system to spatially separate the signal and noise and consequently enables better speech understanding [42] [44].

$$\mathrm{BILD}_X = \mathrm{SRT}_{\mathrm{monaural},X} - \mathrm{SRT}_{\mathrm{binaural},X} \quad [\mathrm{dB}] \tag{2.3}$$

where:

- $\mathrm{BILD}(X)$ = Binaural Intelligibility Level Difference at position X
- $\mathrm{SRT}_{\mathrm{monaural_X}}$ = Speech Reception Threshold monaural fitting at position X item $\mathrm{SRT}_{\mathrm{binaural_X}}$ = Speech Reception Threshold binaural fitting at position X

2.3.1 Swedish Matrix (Hagerman) Test

The Swedish Matrix (Hagerman) Test was used is a very common procedure in audiological diagnostics to access speech intelligibility in noise. It measures the Speech Reception Threshold (SRT), the Signal to Noise Ratio, at which 50 % of the spoken words are correctly identified by the listener. It consists of 20 nonsense sentences, each following a fixed syntactic five-word structure, such as "Anna har tre nya bollar". At the start, the speech signal and background noise are presented at the same level (65 dB). As the test progresses, the speech level is automatically adjusted according to the participant's responses until the 50% threshold is reached. The background noise is a stationary speech-shaped noise that has the same long-term average spectrum as the test sentences to provide uniform masking. The closed-set response format was chosen, in which participants selected their answer from a list of 50 possible alternatives displayed on a screen. This method has been validated and yields results comparable to the open-set version, in which participants repeat the words they understood, and the investigator marks the words correctly identified [45]. A study revealed only a small difference (< 0.5 dB) between the open and closed versions, whereas a stronger influence on the SRT Scores was observed between the different types of maskers [46].

2.4 Digital Signal Processing

A signal can carry various types of information, depending on its origin. Some signals, such as speech, can be wanted or even necessary while some others remain unwanted and therefore disruptive. The latter is then considered as noise. In acoustics, those audio signals originate in pressure variations in the air, which cause oscillations of the surrounding air particles and ultimately form sound waves. These pressure differences over time can be captured by a transducer, such as a microphone, and converted into an electrical voltage. This resulting signal can then be decoded into characteristics of the signal, such as the amplitude (intensity) and the frequency components. At this stage, digital signal processing (DSP) becomes essential, providing precise manipulation and interpretation of audio signals. With the help of a DSP Software such as MATLAB, important aspects of the signal can be enhanced while undesired components such as noise can be suppressed [47], [48]. The following section introduces a technique for extracting meaningful information from a digital audio signal by calculating the frequency response function, as well as a way of manipulating the signal to achieve a new desired outcome.

2.4.1 Windowing

In digital signal processing, signals are often analyzed by dividing them into segments of a chosen window length and processing each segment individually. If the window length does not align with the period of the signal frequency, as illustrated in Figure 2.7, the segment may be cut mid-cycle. This introduces a phenomenon known as spectral leakage. Applying a window function such as the Hann (Hanning) window shown in Figure 2.8 reduces the amplitudes towards the start and the end of the segment. This minimizes discontinuities and thereby improves the accuracy of the transformation from the time domain to the frequency domain [47].

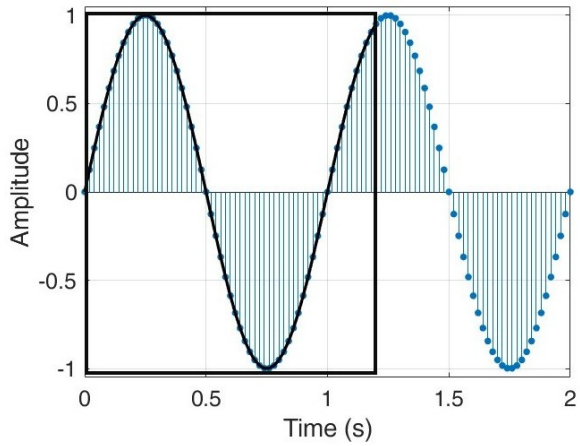

Figure 2.7: Plot of 1 Hz sine wave with a window length of 1.2 seconds indicated.

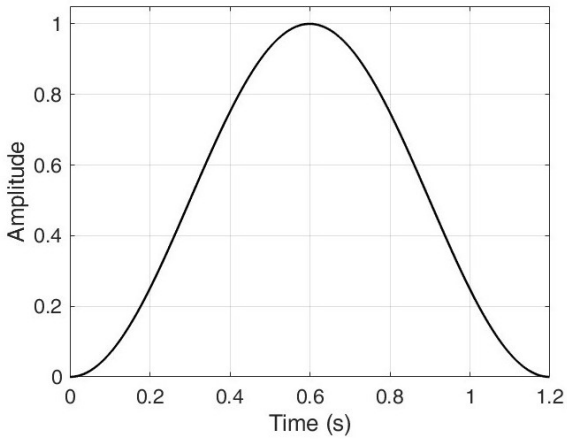

Figure 2.8: Plot of the Hann window function of length 1.2 seconds.

2.4.2 Frequency response function

A force applied to a structure can induce vibrations that manifest in different ways. They may be felt directly by a person in contact with the structure and may cause discomfort. They may be heard when the surrounding air particles are excited or may propagate into connected structures, potentially leading to damage. Understanding how a system responds to applied forces is therefore crucial, as it enables the reduction of unwanted vibrations, for example, through the strategic placement of damping materials or by eliminating the source [49]. Not all vibrations are undesirable, however. In certain cases, such as bone conduction hearing, vibrations are intentionally utilized to compensate for conductive hearing losses [50]. For the sake of simplicity, the head simulator is identified as a linear time-invariant (LTI) system and can therefore be characterized by its impulse response $h(t)$. Linearity implies that the system obeys the superposition theorem, which means that the response to a sum of inputs $x(t)$ equals the sum of the individual responses $y(t)$. Time invariance means that a time shift introduced to the input produces the same time shift in the output [47]. As illustrated in Figure 2.9, analyzing the relationship between the input signal $x(t)$ and the output signal $y(t)$ provides valuable insights into the vibrational behavior of the system, and by knowing the impulse response, one can predict the system's output for any given input signal in the time domain.

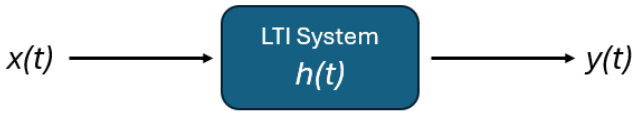

Figure 2.9: Block diagram of a time-invariant system.

c

$$H_{xyz} = \frac{A_{xyz}}{F} \tag{2.4}$$

where:

- H_{xyz} = Frequency Response Function
- A_{xyz} = Complex acceleration frequency function (output)
- F = Complex force sensor frequency function (input)

The equation 2.4 itself is a simplified expression of the FRF estimation for capturing the frequency content. Indeed, there are more steps beforehand necessary, which will be presented in the next section.
First, the signal itself must be divided (sampled) into blocks with a specified block length. Each sample of the original signal $x[n]$ is then multiplied by a window function such as the Hanning window (equation 2.5) to avoid spectral leaking.

$$Y[n] = X[n] \cdot W[n] \tag{2.5}$$

where:

- $X[n]$ = Original sampled signal
- $Y[n]$ = Windowed signal
- $W[n]$ = Window function (Hanning window)
- n = Discrete time index

Next, the Fourier transform is applied to convert both the input and output signals from the time domain to the frequency domain. After the transformation, the signal is multiplied with its complex conjugate to calculate the power spectral density S_{xx} (equation 2.6) at each frequency bin f_n. This function gives information about the energy distribution of the signal across frequencies. The number of averages helps to minimize the "random error", which can occur due to measurement noise [51]. The cross-power spectral density (CPSD) $S_{yx}(f_n)$ can be calculated by multiplying the frequency bin f_n output $Y(f_n)$ with with the complex conjugate of the input $X^*(f_n)$ (equation 2.7) and indicates how the energy distribution of the output correlates with the input energy distribution. The frequency response function $H(f_n)$ can now be obtained by dividing the cross-power spectral density $S_{yx}(f)$ by the auto-power spectral density $S_{xx}(f)$ as shown in equation 2.8 [52].

$$G_{xx}(f_n) = \sum_{1}^{N_{\text{avg}}} X(f_n) \cdot X^*(f_n) \tag{2.6}$$

where:

- $G_{xx}(f_n)$ = Auto power spectral density of the input signal
- $X(f_n)$ = Fourier transform of the input signal at frequency f_n
- $X^*(f_n)$ = Complex conjugate of $X(f_n)$
- N_{avg} =Number of averages in the spectral estimation

$$G_{yx}(f_n) = \sum_{1}^{N_{\text{avg}}} Y(f_n) \cdot X^*(f_n) \tag{2.7}$$

where:

- $G_{yx}(f_n)$ = Cross power spectral density between the output and input signals
- $Y(f_n)$ = Fourier transform of the output signal at frequency f_n
- $X^*(f_n)$ = Complex conjugate of $X(f_n)$
- N_{avg} = Number of averages in the spectral estimation

$$H(f_n) = \frac{G_{yx}(f_n)}{G_{xx}(f_n)} \tag{2.8}$$

where:

- $H(f_n)$ = Frequency Response Function (FRF) at frequency bin f_n
- $G_{yx}(f_n)$ = Cross-power spectral density between output and input signals
- $G_{xx}(f_n)$ = Auto-power spectral density of the input signal $X(f_n)$

2.4.3 Digital Filter

As previously noted, by knowing a system's impulse response in the time domain $h(t)$ or the frequency response function $H(fn)$ in the frequency domain, one can predict its behavior. Consequently, by customizing the impulse response and convolving it with the output signal, the system's response can be shaped in a certain way to fulfill the specific goals of this project. In this thesis, the goal, among other steps, is to adjust the simulator's output so that it aligns with the auditory threshold of the listener. To achieve this, a digital filter is required that not only shapes the amplitude response but also preserves the temporal characteristics of the signal. This can be accomplished by applying a Finite Impulse Response (FIR) Filter. Figure 2.10 illustrates the feedforward path of a first-order FIR Filter. The first path is the direct path, where the input $x(n)$ is being multiplied by the coefficient a_0. The second path introduces a one-sample delay to the signal, denoted by z^{-1}, before multiplying it by the coefficient a_1. By choosing the right coefficients, one can amplify or attenuate certain frequencies depending on the desired outcome. In the end, the contributions of each pathway are summed to produce the new output signal $y(n)$. The more pathways and coefficients the filter contains, the more detailed and complex the manipulation of the input signal becomes at the expense of higher computational costs [53].

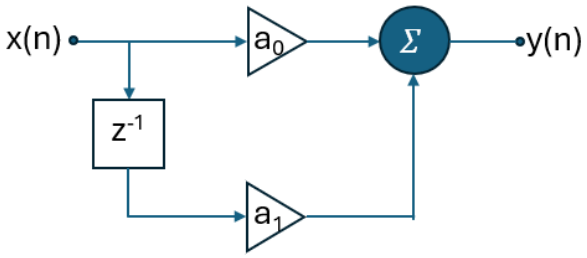

Figure 2.10: Block diagram of a FIR filter with a single sample shift z^{-1} of the signal and its components. [54].

It is possible to distinguish between Finite Impulse Response (FIR) and Infinite Impulse Response (IIR) filters, each offering unique advantages and limitations depending on the application. FIR filters rely solely on a finite number of input samples and do not incorporate feedback from past outputs. As a result, they are inherently stable and typically exhibit a linear phase response, which preserves the shape of the signal. In contrast, IIR filters are more complex. It has a feedback structure, meaning each output depends not only on current and past inputs but also on previous outputs. If not carefully designed, this feedback can lead to instability, where the output grows uncontrollably. Additionally, IIR filters often have a non-linear phase response and are asymmetric, which makes them inappropriate for this thesis. Despite these challenges, IIR filters can be highly efficient, achieving desired filtering characteristics with significantly lower computational cost compared to FIR filters [54].

3
Methods

In this chapter, the method for evaluating the transcranial attenuation of the head simulator is presented, followed by an analysis and comparison of the results with existing literature. To enable live listening to the head simulator's output via headphones, a threshold-matching procedure is performed. As a final step to validate the head simulator's performance, a listening experiment is conducted, and the results are compared with published data. Furthermore, the aim is to investigate the potential benefits of binaural fitting over unilateral configurations in general. The following software tools were used throughout this thesis workflow: Microsoft Excel for data organization and analysis, MATLAB for signal processing and visualization, Microsoft PowerPoint for figure preparation, SigmaStudio for digital signal processing configuration, and AI-based assistants (ChatGPT and Microsoft Copilot) for language polishing, figure generation, and LaTeX formatting support.

3.1 Measurement Setup

Before proceeding with further work, it is essential to evaluate the applicability of the head simulator. This evaluation is performed by measuring the transfer function (H1), according to the Cochlear® Technical Report and calculating the degree of vibration attenuation as it propagates to the contralateral accelerometer. After calibrating the reference force source using a PCB 208C01 force sensor, the transducer was mounted on the head simulator at the same positions where the bone conduction hearing aids are typically placed (see Figure 3.1). A logarithmic chirp stimulus in the frequency range of 100 Hz to 20000 Hz and an amplitude of 0.1 Vrms is introduced for 30 s. Each measurement was repeated five times, with the reference excitation force being detached and reattached before every trial to ensure consistency and account for variability in coupling. The sensitivity of the head simulator was calculated with the formula shown in Equation (3.1) and was later used for the threshold matching procedure.

$$\text{Sensitivity} = \left| \frac{\text{Headsim [V]}}{\text{Forcesensor [N]}} \right| \tag{3.1}$$

Since the head simulator is equipped with two accelerometers, each measuring in three axes (x, y, z), the signals from each axis were combined by summing them. To determine transcranial attenuation (TA), the frequency response function of the contralateral side was subtracted from that of the ipsilateral side (Equation 3.2). The resulting data was then compared to findings from a study conducted by Stenfelt, in which TA was measured in 28 participants with unilateral deafness at the bone-anchored hearing implant (BAHI) position [2].

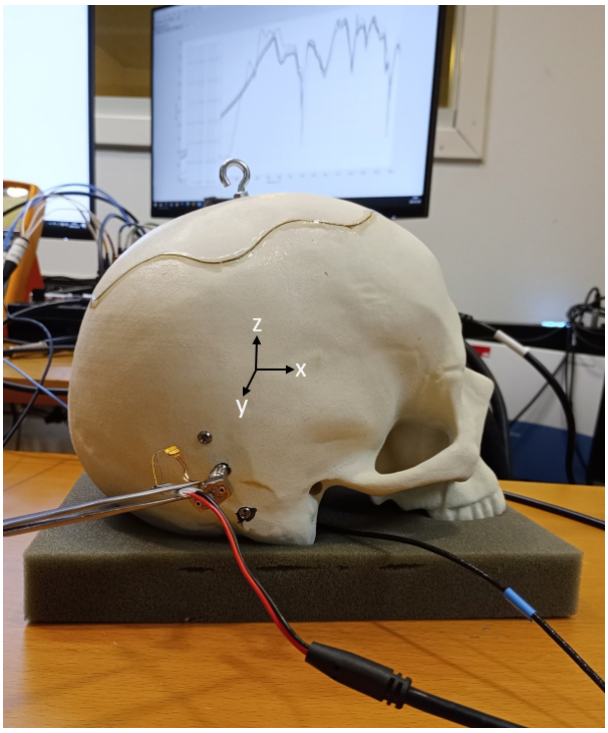

Figure 3.1: A side view of the head simulator Generic during measuring the transfer function.

$$\mathrm{TA} = H1\left(X_{\mathrm{ipsi}} + Y_{\mathrm{ipsi}} + Z_{\mathrm{ipsi}}\right) - H1\left(X_{\mathrm{contra}} + Y_{\mathrm{contra}} + Z_{\mathrm{contra}}\right) \tag{3.2}$$

where:

- $H1$ = Frequency Response Function (FRF) between input force and output acceleration
- X, Y, Z = Complex acceleration frequency components
- ipsi, contra = Ipsilateral and contralateral measurement sides

3.2 Digital Signal Processing

To transform the accelerometer output into a format that simulates the auditory experience of a BAHI (Bone Anchored Hearing Implant) user, digital signal processing was applied. Each step of this process is explained in the following sections. Initially, each axis of the accelerometer is projected onto the excitation force. Afterwards, threshold matching is performed to boost the head simulator's output into the audible range of a human.

3.2.1 Vector projection

As previously mentioned, vibrations along the y-axis are the main contributors to hearing perception, while vibrations in the x- and z-directions have a lower, yet still important, influence. Because the threshold-matching procedure later on amplifies the output into the audible range, a method is required to weight these axes appropriately so that each

axis contributes differently to the overall hearing sensation. This can be achieved using vector projection.
This section describes how each accelerometer axis is projected onto the direction of the excitation force. As shown in Figure A.3, the head simulator includes two red markers indicating the placement of the bone-anchored hearing implant (BAHI). This way, the three-dimensional motion is converted into a one-dimensional vector aligned with the excitation force.

All angles are defined with respect to the normal plane of their associated axis in a three-dimensional Cartesian coordinate system:

- **X-axis angles** are measured relative to the YZ-plane.
- **Y-axis angles** are measured relative to the ZX-plane.
- **Z-axis angles** are measured relative to the XY-plane.

This means that each angle reflects how a directional vector deviates from its normal plane in three-dimensional space. If an angle of 90° is defined for the X-axis, it indicates that the resulting vector points directly along the positive or negative direction of the X-axis itself and is consequently parallel. Directional vectors can be derived from angle values using the cosine function in Equation 3.3 [55]. For this Master's thesis, the equation was adjusted as one can see in Equation 3.4.

$$\text{projected vector} = |A| \cdot \cos(\alpha) \tag{3.3}$$

where:
- $|A|$ = Magnitude of the vector
- α = Angle between the two vectors
- projected vector = Magnitude of the projected vector

$$\text{Vector component}_{(xyz)} = \text{Acc}_{(xyz)} \cdot \cos(90° - \theta) \tag{3.4}$$

where:
- $\text{Acc}_{(xyz)}$ = Triaxial acceleration data along the x-, y-, or z-axis.
- θ = Angle between the axis and its corresponding normal plane.
- $\text{Vector component}_{(xyz)}$ = Projected acceleration component along the direction of the excitation force, used to combine the contributions of each axis into a single effective vector.

As illustrated in Figure 3.2a, projecting vector V onto the Y-axis yields a new vector V' with reduced amplitude, resembling the shadow cast by the original. By projecting each axis onto the excitation force, the relative contributions of the components become clear. Figure 3.2b illustrates the amplitude of each axis within the unit vector. Notably, the Y-axis exhibits the greatest contribution, followed by the X-axis, while the Z-axis contributes the least. The result of $\cos(90° - \theta)$ can be interpreted as a scaling factor that will later be used in programming the DSP hardware. The electrical output of the accelerometers will be multiplied by these factors to align the data with the excitation force. All values can be found in Table A.2.

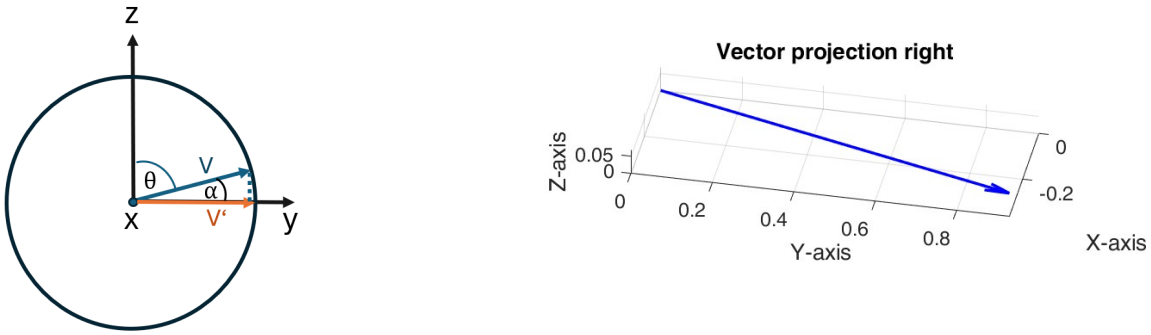

(a) Vector projection of V onto y.

(b) Unit vector after projection onto the excitation force at Baha® position (right).

Figure 3.2: Vector projection onto the excitation force.

3.2.2 Threshold matching filter

Since the accelerometer output does not directly represent how the cochlea responds to vibrations under bone conduction (BC) stimulation, it must be processed to ensure a realistic perceptual experience. To align the thresholds of the two different pathways for bone and air conduction hearing, a threshold-matching procedure implemented as an FIR filter is performed. Given that both pathways produce similar cochlear stimulation, this method can be considered reliable. The MATLAB implementation of this filter is based on code previously used for the previous head simulator. The process involves several key steps. Firstly, all datasets (HL_{BC}, HL_{AC}, $headphonesensitivity$, $headsimulatorsensitivity$) are interpolated to the same frequency grid (250 Hz to 14 kHz) using piecewise cubic Hermite interpolation (pchip). The Gain is calculated based on the following equation 3.5 with $HL_{\text{effective\_BoneConduction}}$ and $HL_{\text{effective\_AirConduction}}$ being explained in Figure 3.3. To translate the physical output of the accelerometer into the actual perceptual loudness, the minimal threshold for conduction stimulation (HL_{BC}) was subtracted from the sensitivity of the head simulator (HS_{Sens}). Additionally, the minimal audible sound pressure level for air conduction (HL_{AC}) was subtracted from the headphone sensitivity (HP_{Sens}) to obtain the effective hearing level.

$$0 = HL_{\text{effective\_BoneConduction}} + Gain + HL_{\text{effective\_AirConduction}} \tag{3.5}$$

where:

- $HL_{\text{effective\_BoneConduction}}$ = Effective hearing level for bone conduction
- $HL_{\text{effective\_AirConduction}}$ = Effective hearing level for air conduction
- $Gain$ = Additional amplification applied to match the effective bone and air conduction levels

To improve the signal-to-noise ration 10 dB was added to the $Gain$. The transfer function was converted from dB to a linear scale and interpolated across the full FFT spectrum. The symmetrical inverse FFT of the full spectrum leads to the desired impulse response. It was centered and truncated to 369 samples, and an hanning window was applied to smooth the filter edges. After convolution of the input signal and the impulse function,

the signal is resampled to the original sampling frequency. Figure 3.3 illustrates the threshold matching, and the variables can be taken from Table 3.1.

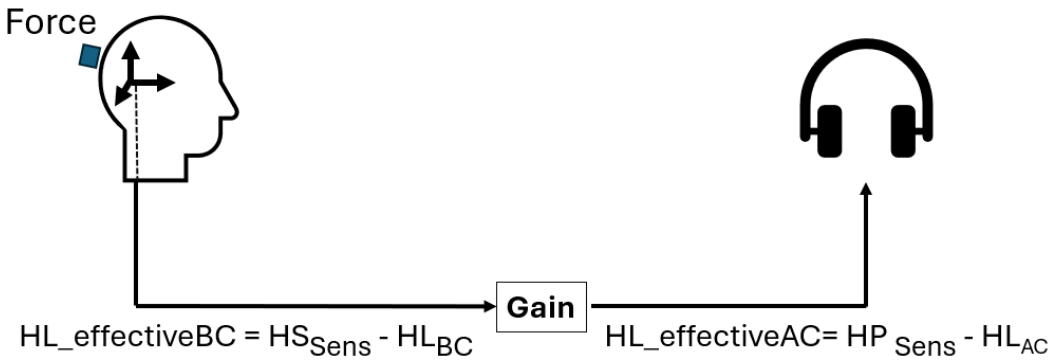

Figure 3.3: Sketch of threshold matching according to the technical report for the Head Simulator

Term	Definition	Unit
HS_{Sens}	Head simulator sensitivity	[V/N]
HL_{BC}	Minimal hearing level for bone conduction [56]	[dBre1N]
HP_{Sens}	Sensitivity of Sennheiser HD650 headphones from data sheet	[dBSPL/1Vrms]
HL_{AC}	Minimal audible sound pressure level for air conduction [57]	[dBSPL]

Table 3.1: Explanation of the variables used for threshold matching.

3.2.3 Live listening

To enable real-time listening with minimal latency and incorporate the threshold-matching impulse response, the digital signal processing unit from a previous master's thesis [58] was reused. It was reprogrammed in SigmaStudio to meet the requirements of the current thesis. The signal path is illustrated in Figure 3.4. Each axis of the head simulator (X, Y, Z) is first projected onto the direction of the excitation force by applying a scaling factor equal to $\cos(\alpha)$. Following this projection, threshold matching is performed to align bone conduction signals with air conduction hearing thresholds. The processed signals from all three axes are then summed, and an additional gain of 10 dB is applied to enhance audibility and signal-to-noise ratio. At the beginning of the signal chain, a high-pass filter (200 Hz) and at the end a low-pass filter (14 kHz) were applied. The final output is a stereo signal suitable for playback through headphones.

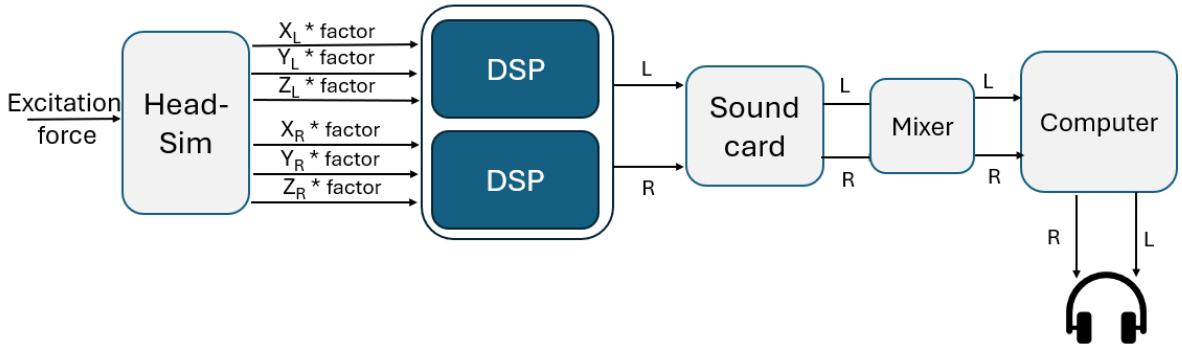

Figure 3.4: Block diagram of the signal path from the head simulator under bone-conducted stimulation to the headphones.

3.3 Listening experiment

At this stage of the thesis, one can listen to the output of the head simulator under BC stimulation, but it is still uncertain whether it realistically replicates the experience of a person treated with a bone-anchored hearing implant. To validate the head simulator's performance, a listening experiment was additionally conducted, and the results were later compared to literature findings. The experiment took place in the listening laboratory at Cochlear Bone Anchored Solution AB in Mölnylcke, Sweden. The laboratory holds a larger acoustically treated room with a speaker array and a control room. To ensure the comfort and safety of participants during the listening experiment, all potential risks were assessed and appropriate mitigation measures identified. The detailed risk assessment can be found in the appendix. All participants were informed beforehand about possible risks, such as e.g., loud sound exposure due to technical failures, as well as fatigue and anxiety, and how those risks are being handled. All employees were invited to the experiment via e-mail and were therefore able to voluntarily schedule a time slot themselves. Only native speaking participants with subjectively normal hearing were included for the listening experiment. Every subject received some sort of compensation in the form of candy.

3.3.1 Calibration

Before starting the trial, a calibration of the whole setup was conducted. A reference microphone was positioned at the center of the loudspeaker array, equidistant at 1.20 meters from each speaker, to calibrate the target sound pressure level of 65 dB. Background noise was measured at a level of 22 dB(A). This was done with the head simulator in the array using two Baha®6 Max Cochlear®. Next, using the Sound Quality and Torso Simulator (Bruel&Kjaer), the total output sound pressure level of the headphones was measured to ensure a consistent level of 65 dB for both signal and noise. This calibration is crucial, as the Speech Reception Threshold (SRT) test begins with a signal-to-noise ratio (SNR) of 0 dB. As a final step, the Baha® In-situ audiogram function was used to verify the linearity after digital signal processing. For this purpose, output measurements were taken at stimulation levels of 30 dB and 40 dB. As shown in Figure 3.5, a 10 dB SPL increase in input level generally resulted in a proportional 10 dB SPL increase across most frequencies. However, deviations from this trend were observed at specific frequencies. For instance, at 2 kHz, a 10 dB input amplification yielded only a 5 dB

increase in output, whereas at 1.5 kHz, the same input gain produced a 14 dB increase. These discrepancies suggest frequency-dependent nonlinear behavior in the transmission system.

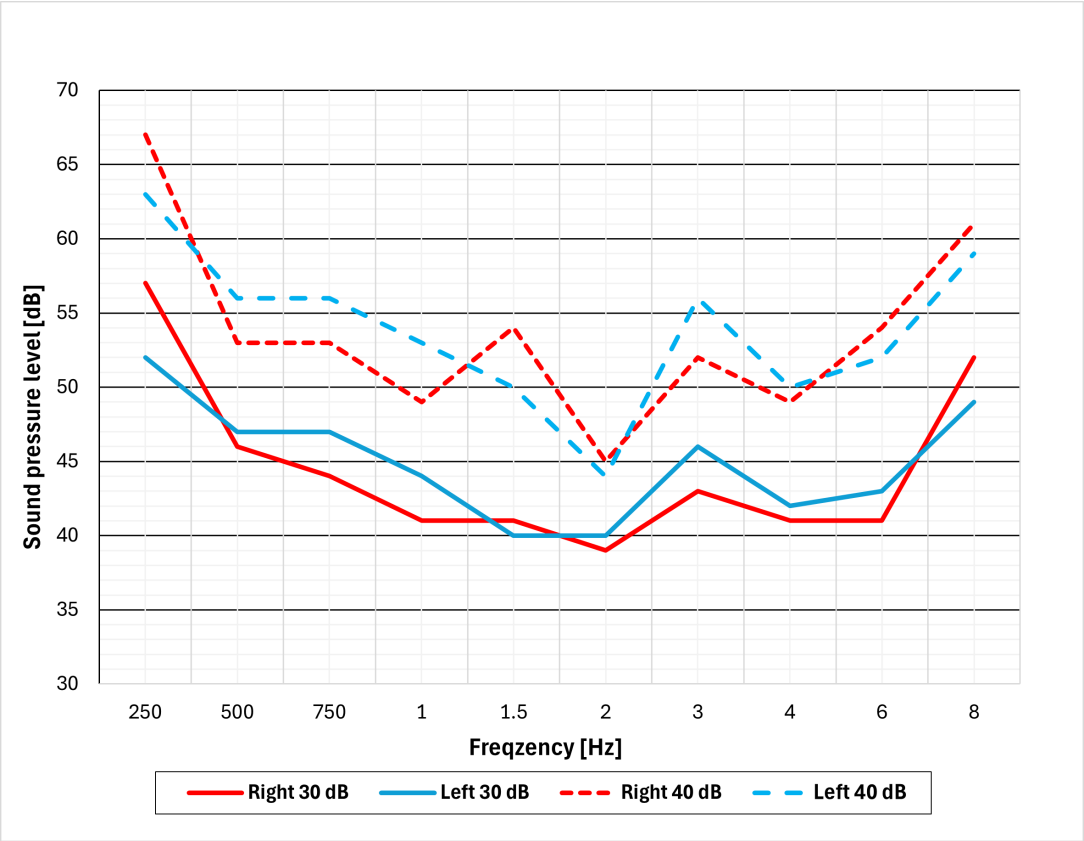

Figure 3.5: In situ measurement of the head simulator output when stimulated via Baha® Insitu audiometry function with stimuli at 30 dB and 40 dB.

3.3.2 Test setup

The head simulator, as one can see in figure 3.6 was positioned in a sound-insulated room between the loudspeaker array on a steel plate with a vibration-isolating interlayer. Sound was processed in the DSP hardware and transmitted to the headphones. The participant was sitting during the test next door, listening to the head simulator's output via headphones. This setup enables a free field measurement without any direct sound from the loudspeakers reaching the participant. The hearing aids were programmed via software to provide a linear 10 dB amplification across all frequencies. To provide true omnidirectional, one microphone on each device was deactivated. All additional features, including feedback control and the classifier (automatic adaptation to the acoustic environment), were additionally disabled. In Figure 3.6 one can see the individual conditions where sound and noise are collocated (S0N0) and spatially separated (S0N270). The second Baha® device was mounted on the contralateral side, away from the noise source, allowing the head shadow effect to enhance speech intelligibility in the presence of background noise.

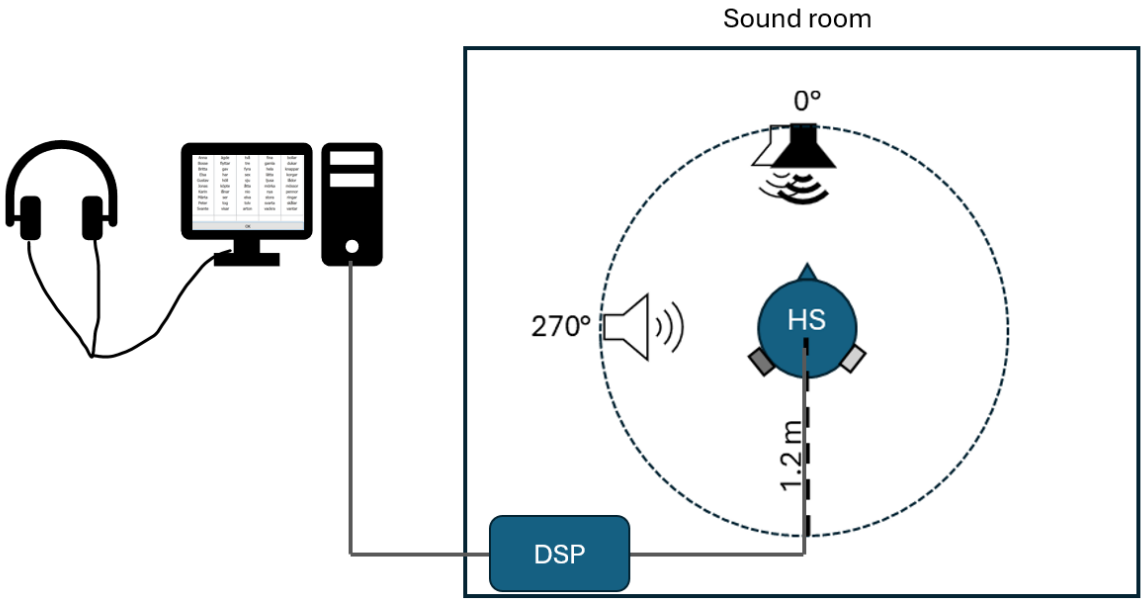

Figure 3.6: Setup for different test conditions with head simulator (HS) in the center of the loudspeaker array in the soundproof room. The black loudspeaker indicates the signal, and the white loudspeaker represents the location of the noise source.

3.3.3 SRT measurement

The SRT measurement was performed under four different setup conditions as presented in Table 3.2. To control for training effects and other factors, the test conditions and sentence sets were randomized. At the beginning, each participant was introduced to the test procedure and completed a short training session of 10 sentences to become familiar with the setting and the sound. The actual SRT measurement then consisted of 20 sentences per session. After each round, participants rated their perceived listening effort on a visual analogue scale, while the investigator prepared the next setup. The scale ranged from 0 (indicating low effort) to 10 (indicating high effort) and the participants were asked to make use of the whole range. During this time, the headphones were removed to prevent any unintended sound disturbances.

Setup	**Description**
S0N0 monaural	Signal and noise presented from the front with one Baha® (left) attached
S0N270 monaural	Signal front, noise from the side with one Baha® (left) attached
S0N0 binaural	Signal and noise presented from the front with two Baha® attached
S0N270 binaural	Signal front, noise from the side with two Baha® attached

Table 3.2: Table of contents for different test conditions.

4

Results

The following presents the results of the frequency response function (FRF) measurements conducted both before and after the threshold-matching procedure. This analysis gives insight if and how the vector projection alters the resulting signal, as well as what the objective outcome is after applying digital signal processing. To establish a reference point, the results obtained using vector projection are compared with those obtained by simply summing the acceleration axes, as well as with the approach proposed by Dobrev et al. [39]. In addition to the objective measurements, a comprehensive statistical analysis of the listening experiment results is presented. This evaluation aims to quantify the perceptual accuracy of the head simulator under bone conduction stimulation and to determine how closely the simulated output matches the auditory experience of a listener.

4.1 Transcranial attenuation

In this section, the analysis of the frequency response when excited from the left side will be displayed only. Corresponding graphs for excitation on the opposite side are provided in the appendix for reference. Figure 4.1 and 4.2 illustrate the frequency response function (FRF) for left-side excitation. For comparison, the responses of each axis, the combined axis, the combined axis calculated using the Dobrev method, and the graphs with all axes projected onto the excitation force are presented.

In the ipsilateral combined graph (4.1b) two distinct dips are observed after vector projection, accompanied by a reduction in amplitude for the X- and Z-axes. On the contralateral side, the combined-axis response without vector projection shows a lower amplitude than the Y-axis in the low-frequency range, for reasons that remain unclear. This effect, however, disappears after vector projection. Aside from these noted differences, the combined-axis results closely match those obtained using the Dobrev method, indicating that they are suitable for further analysis and processing.

Across all graphs, the first skull resonance occurs at approximately 800 Hz, consistent with the behavior of a real human skull. The plots cover the frequency range from 200 Hz to 9.6 kHz, corresponding to the operational bandwidth of the Baha® 6 Max system. However, for reasons unknown, after vector projection, two narrow dips appear in the FRF plot 4.1b at 1.2 kHz and 2.2 kHz. Simply summing the vibrational energy of each axis in the time domain represents a more straightforward but less accurate approach since it tends to produce antiresonances. This behavior arises because certain vibrational components are out of phase or oriented in opposite directions, which can lead to destructive interference.

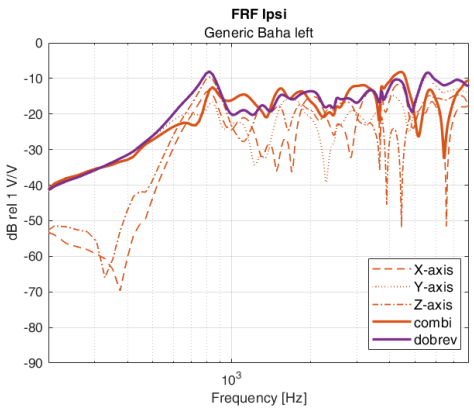

(a) Combined axis

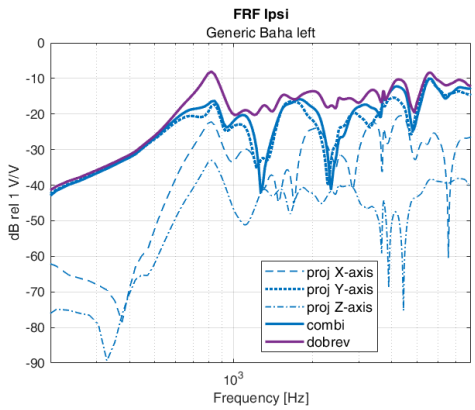

(b) Combined axis with proj. vectors

Figure 4.1: Ipsilateral frequency response function.

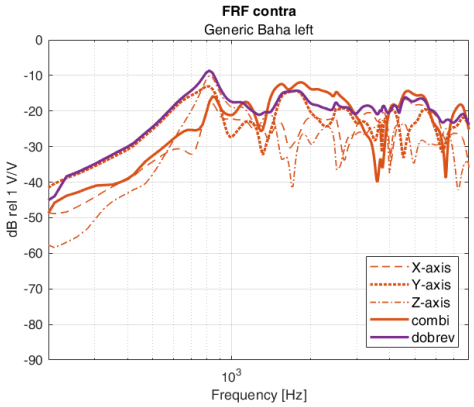

(a) Combined axis

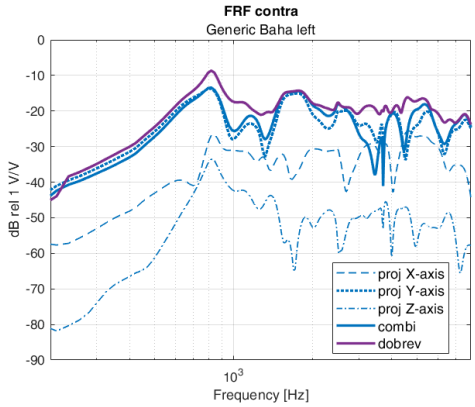

(b) Combined axis with proj. vectors.

Figure 4.2: Contralateral frequency response function

In Figure 4.3 the accumulated phase is plotted and shows the shift of the output signal in comparison to the input signal. As one can see in Figure 4.3 the skull acts below 1 kHz as a rigid body since the accumulated phase response is near-zero, which aligns with the literature [59]. At higher frequencies, where the wavelengths are shorter than the diameter of the skull, the vibrational motion transitions from rigid-body behavior to more complex translational and rotational patterns, resulting in increased phase delay.

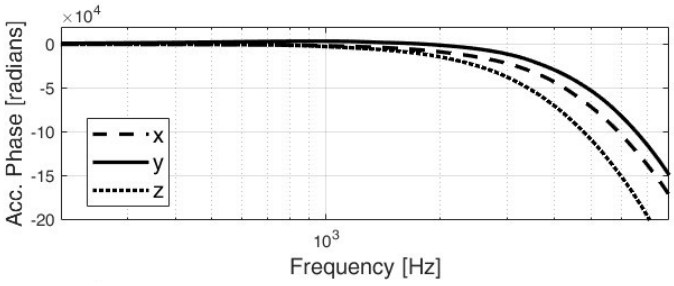

Figure 4.3: Accumulated phase of each axis ipsilateral with excitation force on the left side.

Figure 4.4 shows the transcranial attenuation (TA) calculated in MATLAB using a simple summation of the axes, both before (orange dashed line) and after vector projection (blue line), as well as the TA obtained using the Dobrev method (purple dashed line). The black line represents the median TA of the human skull, based on a study by Stenfelt et al [2], with the dashed lines indicating the standard deviation. Up to approximately 1 kHz, the TA after vector projection remains close to 0 dB - 5 dB, as expected. Two pronounced dips, at around 1.2 kHz and 2.3 kHz, are the result of antiresonances occurring ipsilaterally after vector projection. In the range between 3 kHz and 4.5 kHz, the measured attenuation exceeds values reported in clinical studies, which can be attributed to sharp peaks and dips present in both the ipsilateral and contralateral responses.

correct legend!

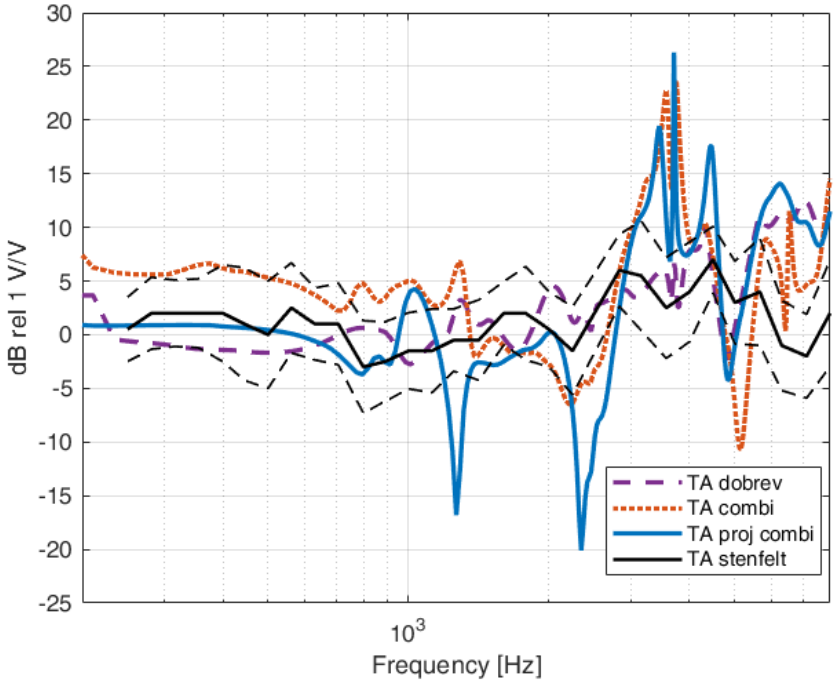

Figure 4.4: Transcranial attenuation with excitation force on the left side.

4.1.1 Threshold matching

This section presents the frequency response obtained after applying vector projection and convolving the signal with the new impulse response. Figure 4.5 illustrates the frequency response function (FRF) for both ipsilateral and contralateral stimulation. Interestingly, for reasons not yet fully understood, the contralateral amplitude is higher than the ipsilateral response below 1 kHz when excited from the right side. Additionally, above 3 kHz, the transmission advantage (TA) is significantly greater than expected. This phenomenon does not occur when excited from the left side. However, when listening through two attached BAHIs, the sound is perceived as centered. This suggests that the signals from both sides are being amplified similarly, resulting in a balanced auditory experience. Narrow spectral dips are observed around 1.2 kHz and 2.1 kHz. While these may affect pure tone perception, they do not appear to influence the overall sound quality or spatial impression.

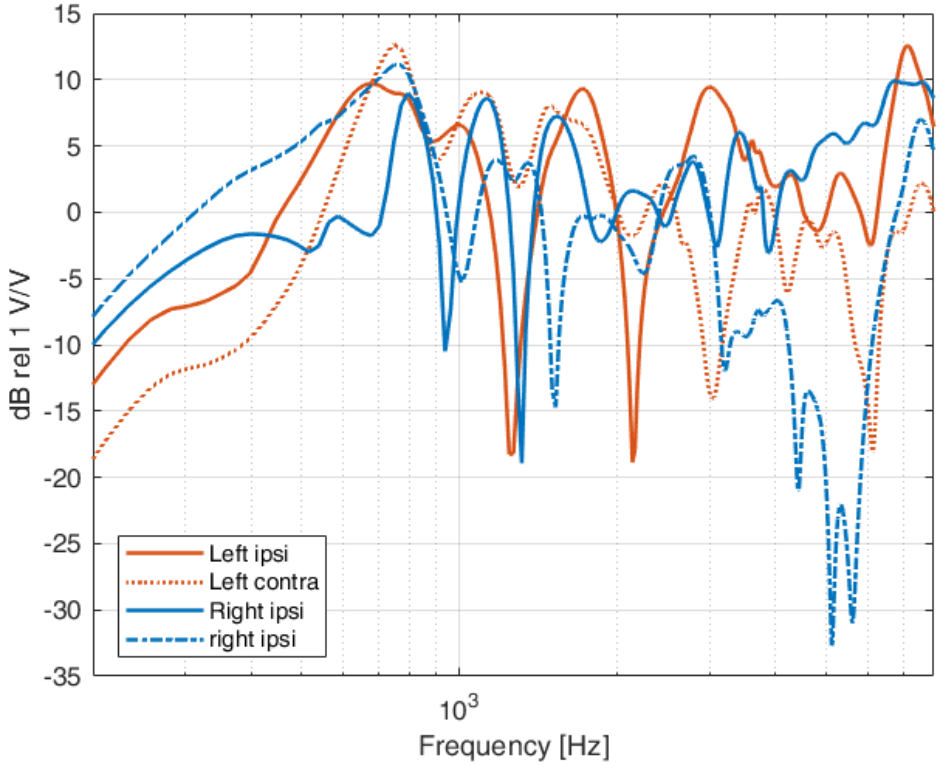

Figure 4.5: FRF after threshold matching.

4.2 Listening Experiment

The following section presents and statistically analyzes the results of the listening experiment. For graphical representation and in-depth data analysis, Microsoft Excel, MATLAB, and IBM SPSS Statistics were used.

4.2.1 Participants

A total of 37 native speakers (20 female, 17 male) participated in the listening experiment, with ages ranging from 18 to 65 years. All participants were employees at Cochlear Bone Anchored Solutions AB, and each reported subjectively normal hearing. No audiometric testing was conducted to verify hearing thresholds, as such data are considered sensitive and were not collected for this listening experiment. Figure 4.6 illustrates the age distribution of the sample. Notably, only a small proportion of participants fell within the youngest (18–30 years) and oldest (60–65 years) age brackets, while most participants were between 31 and 60 years old.

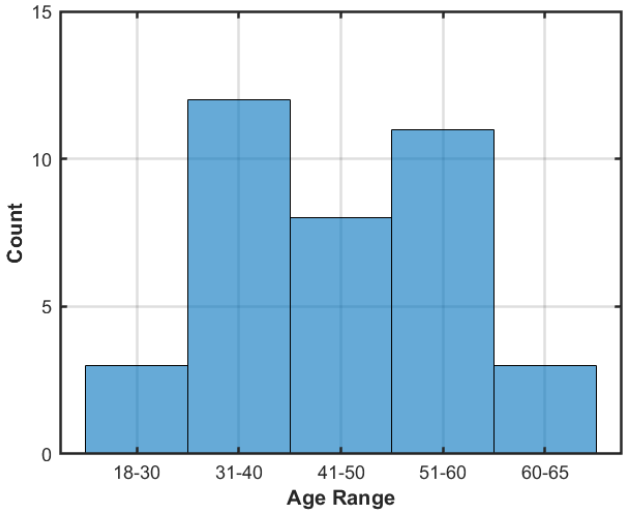

Figure 4.6: Age distribution of participants.

4.2.2 SRT scores

Before proceeding with the statistical analysis, an initial overview of the data is provided in Figure 4.7 and Figure 4.8. Additionally, the data were compared against clinical data from other listening experiments involving normal-hearing test subjects. The studies vary in age span, number of participants, and test conditions, and should therefore only be considered as a rough point of reference to verify the performance of the head simulator itself. Unfortunately, only studies involving binaural fitting met the criteria for meaningful comparison with the present data, and no comparison for the S0N0 mono and S0N270 mono setup was possible. Figure 4.7 illustrates the SRT scores in the form of error bars, which represent the sample mean and individual standard deviation. The exact values are provided in Table 4.2.
The setup where noise and speech were collocated led to an extraordinarily good SNR (-10.78 dB $\pm$ 0.97). When comparing the value to literature findings, where an SNR of

typically - 8 dB is stated, one can conclude that the speech intelligibility in noise of the participants was approximately 3 dB better than expected. This finding will be examined later on in the discussion part. The setup S0N270 differs from the other conditions with a mean of -14.40 dB ($\pm$ 2.15) and will later on be checked for significance.

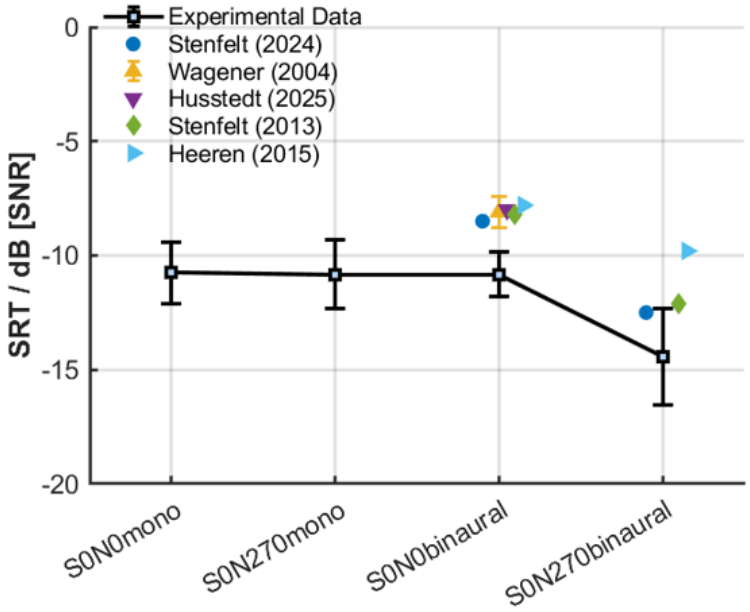

Figure 4.7: Speech reception threshold (SRT) for different test conditions [60][61][62][63][64].

In figure 4.8 it is illustrated how the speech reception threshold (SRT) improves with spatial separation of sources (ILD) and going from monaural to binaural fitting (BILD). The monaural fitting seems to lead to no improvement when the signal is presented from the front and noise from the side. This is reasonable since the noise is on the same side as the activated Baha®, leading to direct masking. If the Baha®, contra laterally to the noise, was activated, the listener could make use of the head shadow effect and therefore have better speech understanding. In binaural fitting, however a increased speech understanding in noise was achieved by a 3.62 dB ($\pm$ 1.78). This indicates how the participants could make use of the spatial cues when the sources were separated. For the comparison of binaural and monaural fitting with spatial source separation (BILD), an average benefit of 3.58 dB ($\pm$ 1.52) was observed. These findings align closely with clinical data from normal-hearing individuals, as the observed mean values correspond well with those achieved in the listening experiment. When both speech and noise originated from the front, no measurable improvement in speech understanding was observed with the addition of a second hearing aid. The standard deviation for ILD Binaural and BILD S0N270 shows a moderate inter-individual standard deviation, which can also be found in other studies, as one can see in the plot [65]. The results of the questionnaire assessing perceived mental effort—rated on a scale from 0 (very low effort) to 10 (very high effort) are presented in Figure 4.11 and in Table 4.2. The mean values for each condition range between 6.70 and 6.94, indicating that all rounds were perceived as the same amount of moderately difficult.

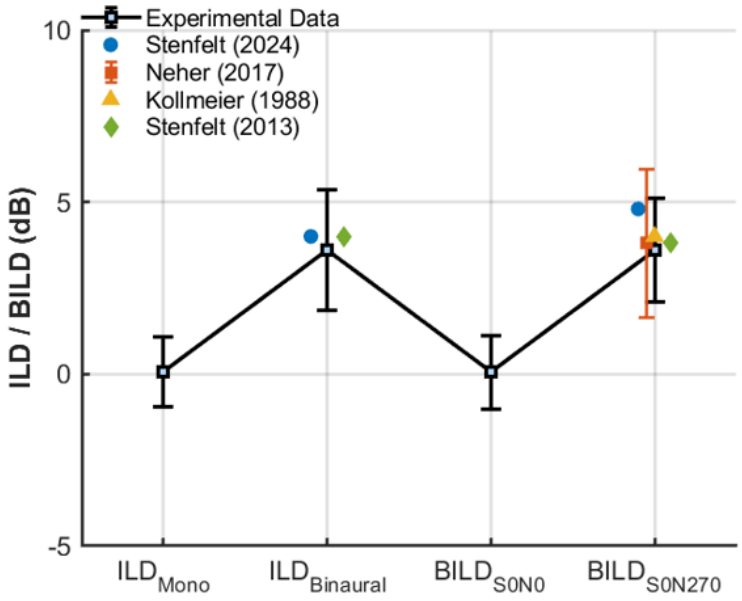

Figure 4.8: ILD and BILD for different test conditions[60][61][66][67][63].

4.2.3 Statistical analysis

To assess the distribution of the data and evaluate normality versus non-parametric characteristics, box plots were generated. These visualizations, presented in Figure 4.9 and Figure 4.10, provide an overview of central tendency, variability, and potential outliers. The box plots display the median, represented as a bold horizontal line, along with the lower and upper quartiles of the data distribution, and outliers are marked as a plus sign (+). Notably, only the configuration involving bilateral bone-anchored hearing implants (BAHIs) with spatially separated sources (S0N270binaural) deviates from the other conditions with a median of -15.1 dB and interquartile values ranging from -15.7 dB to -13 dB. The fact that the median is in the lower half of the boxplot indicates a skewness of the data. Whiskers being longer than the boxplot itself show a high variability of the data, which can especially be seen in the boxplot for the S0N270 setup (4.9) and in the ILD / BILD results.
When interpreting the statistical results, it is essential to account for certain effects, such as age or order of presentation, that could influence the overall performance. To minimize the training or adaptation effects, all conditions and stimuli were presented in a randomized order. Given that age can influence the ability to understand speech in noise, this variable was specifically considered. To ensure age-related homogeneity while remaining a sufficiently high sampling number (N>10) with statistical power, two groups were created, ranging from 18-50 and 51-65. This decision was based on comparing the mean values of each age group and the individual standard deviation. Since the data in general was found not to be normally distributed, non-parametric tests were utilized for statistical analysis. To examine significant differences across the four test conditions, a Friedman test was performed, followed by a Post hoc analysis.

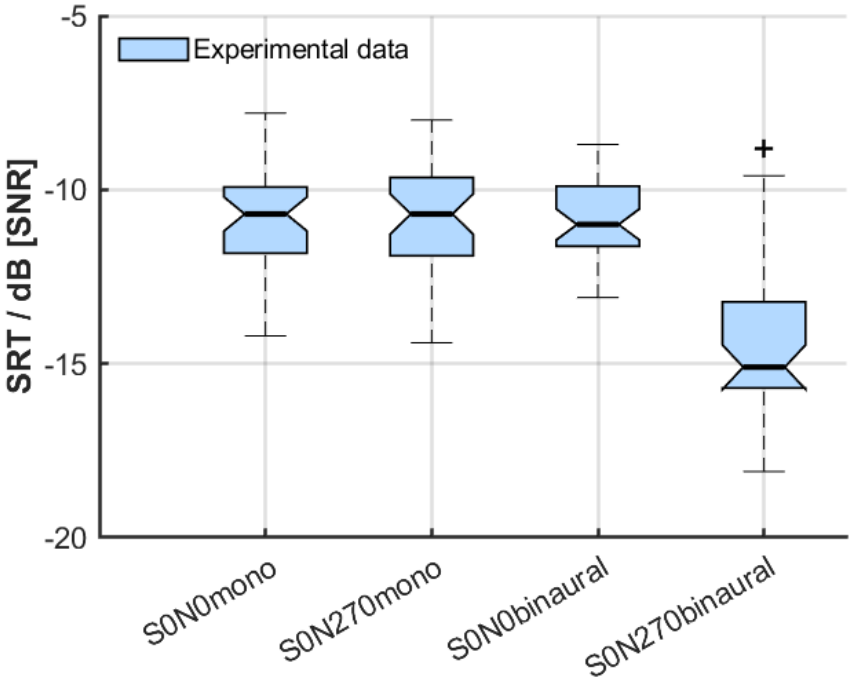

Figure 4.9: Box plot with Speech reception threshold (SRT) for different test conditions.

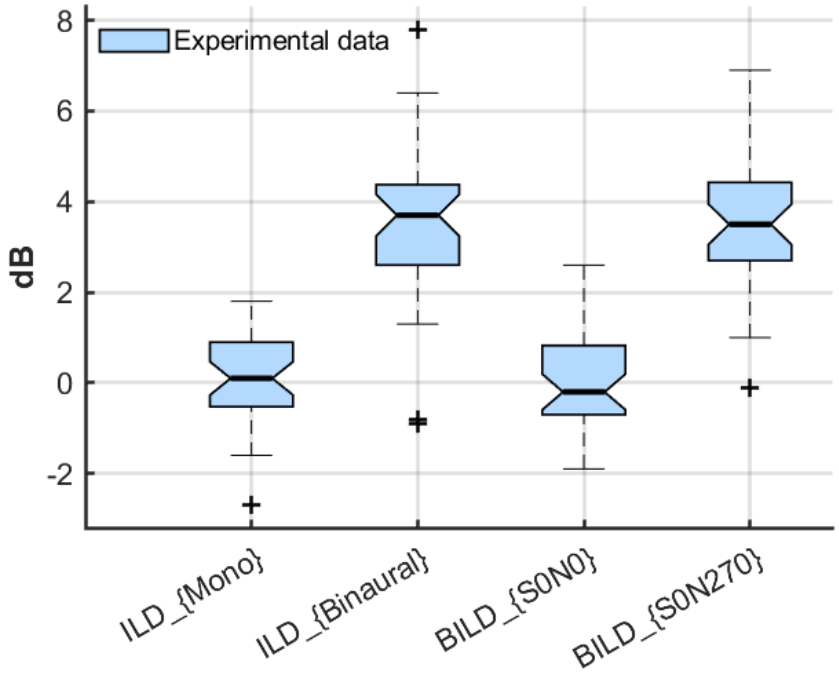

Figure 4.10: Boxplot with ILD and BILD for different test conditions.

A Friedman test was conducted to assess differences across the four test conditions. The analysis included 37 participants and revealed a statistically significant effect, $\chi^2(7) = 235.92$, $p < 0.001$, indicating that at least one condition differed meaningfully from the others in terms of performance. The post hoc analysis with the Wilcoxon signed-rank test and Bonferroni correction showed a significant difference ($p<0.001$) of the setup where sound was coming from the front and noise from the side with two Baha®'s attached (S0N270 b) compared to all the other conditions. Consequently, the participants were able to achieve a better SNR due to the spatial cues provided by the binaural fitting.

The Mann–Whitney U test showed differences in SRT scores between the two age groups over all test conditions. However, due to the sensitivity of the data and the potential conclusions one could draw, these findings will not be discussed further. Instead, the analysis will focus on relative measures such as ILD and BILD. The results of the statistical comparisons are summarized in 4.1 where m denotes monaural and b denotes binaural conditions. With Equation 4.1 the effect size r can be calculated to interpret whether the observed differences are big or rather negligible. An r value above ± 0.5 indicates a substantial difference, which can also be seen when comparing setup S0N270 binaural to the other arrangements [68].

$$r = \frac{Z}{\sqrt{N}} \tag{4.1}$$

where:

- r = Effect size, representing the magnitude of the observed effect.
- Z = Standardized test statistic obtained from the Mann–Whitney U test.
- N = Total number of subjects included in the analysis.

Table 4.1: Statistical analysis for the effect of the test conditions

	S0N270 m - S0N0 m	S0N0 b - S0N0 m	S0N270 b - S0N0 m	S0N0 b - S0N270 m	S0N270 b - S0N270 m	S0N270 b - S0N0 b
Z	$-,500^b$	$-0,181^b$	$-5,266^b$	$-0,066^b$	$-5,289^b$	$-5,258^b$
Asymp. Sig. (2-tailed)	0,582	0,856	$< 0,001$	0,948	$< 0,001$	$< 0,001$
r (N=37)	-0.08	-0.03	-0.85	-0.01	-0.86	-0.86

[a] Wilcoxon Signed Ranks Test

[b] Based on positive ranks.

Table 4.2: Mean and Standard Deviation (SD) values for each listening condition and the ILD / BILD and rating of the mental effort

Listening Setup	**SRT / SNR [dB]**	**SRT / SNR [dB]**			**Rating [1–10]**
	Mean ± SD	**Median**	**min**	**max**	**Mean ± SD**
S0N0 mono	-10.76 ± 1.34	-10.70	-11.83	-9.93	6.87 ± 1.85
S0N270 mono	-10.82 ± 1.53	-10.70	-11.90	-9.65	6.74 ± 1.95
S0N0 binaural	-10.82 ± 0.97	-11.00	-11.63	-9.90	6.70 ± 1.95
S0N270 binaural	-14.42 ± 2.15	-15.10	-15.74	-13.23	6.94 ± 1.82
ILD Mono	0.07 ± 1.02	-0.10	-0.53	0.90	–
ILD Binaural	3.62 ± 1.78	3.70	2.6	4.38	–
BILD S0N0	0.06 ± 1.07	-0.20	-0.70	0.83	–
BILD S0N270	3.58 ± 1.52	3.50	2.7	4.43	–

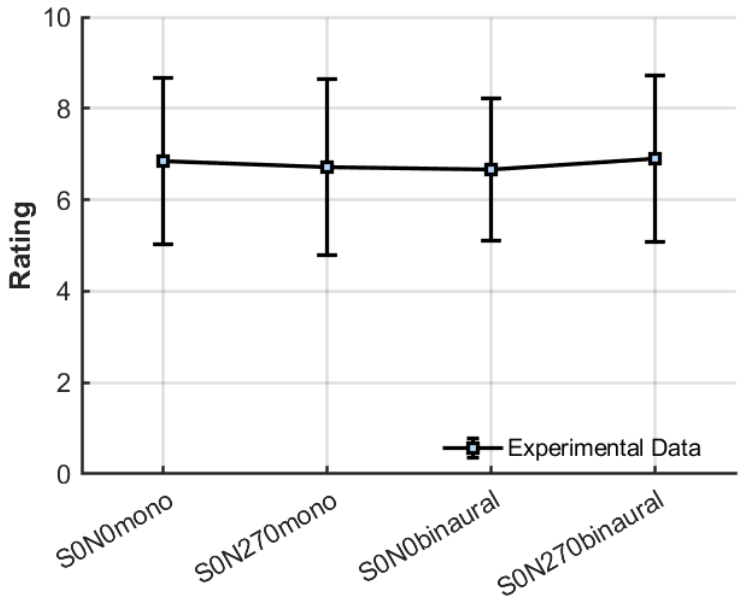

Figure 4.11: Plot with mean and standard deviation of the questionnaire ratings.

5
Discussion

The head simulator is an approach to mimic bone conduction behavior on a real human skull; it cannot fully replicate the physiological conditions. This is because there are facial parts missing, which have an impact on the overall transmission of vibrational energy. Additionally, there are multiple screws integrated in the skull for different positioning of the BAHI. Since these screws are smaller than the wavelengths within the frequency range of interest, and the overall mass of the simulator, they are considered to have a negligible affect the frequency response function.

Although the frequency response functions appear reasonable, it is important to recognize that the vibrational behavior was calibrated under single-source excitation. Introducing two simultaneous excitation forces may result in a different vibrational pattern, as the signals captured by each accelerometer represent a superposition of the ipsilateral excitation and the contralateral transmission, attenuated and phase-shifted in a frequency-dependent manner. The impact of this superposition on the overall output remains uncertain and needs to be studied in further investigations. Nevertheless, linear behavior is still assumed.

The loudspeaker output calibration was conducted using a single microphone positioned at the center of the loudspeaker array. As the head simulator was positioned on a steel plate with a layer of vibration-isolating material, acoustic reflections may have influenced the resulting sound pressure level. To investigate this further, additional measurements were conducted using various fixation methods for the head simulator. These tests revealed no significant differences in the frequency response. Even if minor influences were present, they would likely affect all measurement conditions equally.

In terms of sound quality, the head simulator performed reliably at output levels below 80 dB SPL. Beyond this threshold, signal distortion occurred due to the sound card reaching its performance limit. Nevertheless, as the listening experiment was designed to remain below 65 dB SPL, this limitation was considered negligible. The volume control of the mixer was adjusted to a level that ensured clear audibility while keeping background noise at a barely noticeable level so it would not interfere with the SRT measurement, which involved additional noise exposure. It appeared that the speaker array distorts for the Matrix test above 80 dB. It was known that the DSP works without distortion when the stimulation is with 0.1 Vrms on the reference actuator. Although linear behavior was assumed, the BC in-situ audiogram (BC Direct) revealed limitations introduced by the DSP, suggesting that a lower amplification level would have been more appropriate.
This residual noise may have originated from quantization errors, filter artifacts, or limitations in the dynamic range of the sound card and hardware. To address this issue, further investigation would be needed.

The in situ audiogram function of the Baha® system demonstrated nonlinear behavior, as an amplification of 10 dB did not yield a uniform increase in sound pressure level across all frequencies. Instead, certain frequency bands exhibited higher or lower amplification. This irregularity may be attributed to antiresonance effects introduced during vector projection and threshold-matching procedures, the skull properties themselves, or the upper limit of the DSP was reached, and no further amplification is possible. Additionally, part of this variability may originate from the frequency response characteristics of the Baha® 6 Max device itself. The extent to which this nonlinear response influenced the outcomes of the listening experiment remains uncertain and requires further measurements.

A filter length of 369 taps was selected as a compromise between achieving sufficient frequency selectivity and maintaining low latency suitable for real-time listening. Subjective comparisons with shorter and longer filter lengths did not reveal noticeable differences in perceived audio quality. However, the influence of filter length on parameters such as group delay and, consequently, the perception of spatial cues, was not systematically investigated. This remains interesting for future research.

Directly summing the vibrational energy across axes in the time domain led to artificial antiresonances, probably caused by phase misalignment and oppositely oriented vector components. This phenomenon would not occur when applying the Root-Sum-of-Squares (RSS) method. While the root sum square (RSS) method is well-suited for calculating the frequency response function (FRF) and visualizing the resultant vector in plots, it leads to only positive magnitudes, making it unsuitable for audio playback, which is the main goal of this thesis. Future work should explore more advanced smoothing techniques for the target curves to achieve a more reliable and representative frequency distribution.
During the implementation of the vector projection within the DSP chain, it was observed that increasing the weighting of the Z-axis resulted in greater amplification in the low-frequency range. Looking at the calibration measurements, one notices clearly that only the y-axis contributes to the signal in the lower frequencies, whereas the X- and Z-axis (not the stimulation directions) pick up nearly no signal. This is expected, as low frequencies induce a motion of the whole head in the direction of the stimulation. Consequently, further measurements are required to determine whether frequency-dependent adjustments after applying the weighting factors are necessary to ensure a realistic bone-conduction hearing simulation.

When looking at the SRT scores of the listening experiment extraordinary low SNRs were reached for each test condition. There is a systematic shift of about 3 dB noticeable, which could be due to the nonlinear behavior of the head simulator after digital signal processing. As one can see in Figure 4.5 there is a decreased amplification in the lower frequency part. This could lead to a better understanding of noise and an overall better SNR. However, since the main focus was on the binaural intelligibility level difference (BILD), which is a relative value, the outcome of the listening experiment is seen as successful. In order to address this issue, measurements and comparisons with the previous head simulator would be beneficial, since reasonable SNRs around -8 dB were reached in a small listening test setting (N=9).

In the statistical analysis, a high variability was detected. This could be due to the

great age span of the participants. Since it is stated that age correlates with the ability of understanding speech in noise, even if hearing is subjectively normal. Additionally, deviations in hearing thresholds can not be excluded even if participants stated normal hearing. However, due to the high number of participants, this issue should not impact the results. For further studies, where the SRT scores alone are in focus, the age span should be limited and probably not exceed the age of 40. Under different circumstances, the hearing threshold of each participant should be measured, and the pure tone average (PTA) displayed to ensure a homogeneous test group. Since in this study the benefit of binaural hearing was of interest, a wider age range was chosen to display a more general trend and reach a greater number of participants.

To avoid exceeding the participant's cognitive capacities, it was recommended that no more than five test runs should be completed per individual. As only four test conditions were measured, an additional run was reversed for cases in which the SRT threshold could not be determined. Fortunately, it only occurred four times that a test round had to be repeated. Several participants reported feeling mentally fatigued afterward. To mitigate factors such as fatigue and training-related improvements, the test conditions were randomized. Notably, some participants struggled to recall the word while simultaneously trying to find it on the response matrix displayed on the screen. This represents a disadvantage of the closed-set test format compared to the open-set version, where the participant repeats the word understood, and the investigator notes correct responses in the system. Nevertheless, it was still the most practical solution, particularly since the investigator was not a native Swedish speaker.
The questionnaire for rating how high the mental effort was to complete the tasks had mainly the purpose of keeping the participants occupied while the setup was rearranged. Overall, the results did not reveal any consistent subjective differences between test conditions. However, several participants noted that the configuration reaching the best SNR initially felt easier but became more challenging toward the end. This observation is plausible, as the SNR decreased over time, thereby increasing listening difficulty. In hindsight, to better investigate the subjective benefit of binaural fitting, a dedicated test run could have been implemented in which participants completed only three rounds per condition, with a specific emphasis on mental effort.

In clinical audiology, the test configurations S0N0 and S0N270 are widely used and offer a controlled framework for isolating the effects of monaural and binaural fittings. These setups are considered sufficiently robust for validating the performance of the head simulator under standardized conditions. For future investigations with more complex scenarios, such as frontal speech presentation combined with diffuse noise fields, may be employed to simulate more real-life scenarios.

6
Conclusion

This Master's thesis aimed to further develop the new anatomical head simulator for the perception of complex real-life scenarios through bone conduction stimulation. It is challenging to precisely replicate the three dimensional cochlea response to bone conduction stimulation, since not all mechanisms are fully understood. The vector projection approach explored in this work was designed to align with previous experimental findings, which suggest that the cochlea is particularly sensitive to vibrations coming from a specific direction.

The transcranial attenuation, which is defined as the reduction in vibrational energy propagating from the ipsilateral to the contralateral side of the head, was calculated and found to range between 0 dB and 5 dB in the low-frequency region, with attenuation increasing at higher frequencies. These findings are consistent with existing literature on bone conduction transmission.

In summary, the results of the listening experiment successfully showed that there is a benefit of binaural fitting. Since the outcome of the ILD and BILD align with the literature, one can conclude that the way the head simulator is working is in a reliable way. The SRT score improvements when switching to two bone conduction hearing aids show that the participants were able to make use of the spatial cues, leading to an overall better speech intelligibility when both sources are separated. However, the accuracy of sound quality and frequency-dependent amplification cannot be fully guaranteed and requires more investigation. Another listening experiment where individuals with unilateral bone conduction hearing aids evaluate the sound quality could provide valuable insights into the accuracy of bone-conducted stimulation. Future research may focus also focus more specifically on spatial perception, particularly how accurately participants can localize sound sources. For now, the ability of the head simulator to replicate binaural hearing and processing through headphone playback presents exciting opportunities for future product testing and new applications.

Bibliography

[1] Stefan Stenfelt. "Bilateral fitting of BAHAs and BAHA fitted in unilateral deaf persons: acoustical aspects". In: *International Journal of Audiology* 44.3 (2005), pp. 178–189. DOI: 10.1080/14992020500031561.

[2] Stefan Stenfelt. "Transcranial Attenuation of Bone-Conducted Sound When Stimulation Is at the Mastoid and at the Bone Conduction Hearing Aid Position". In: *Otology & Neurotology* 33.2 (2012), pp. 105–114. DOI: 10.1097/MAO.0b013e31823e28ab.

[3] World Health Organization. *Deafness and hearing loss*. https://www.who.int/news-room/fact-sheets/detail/deafness-and-hearing-loss. Abgerufen: 22. September 2025. 2025. URL: https://www.who.int/news-room/fact-sheets/detail/deafness-and-hearing-loss.

[4] M. L. Cantuaria et al. "Hearing Loss, Hearing Aid Use, and Risk of Dementia in Older Adults". In: *JAMA Otolaryngology–Head & Neck Surgery* 150.2 (2024), pp. 157–164. DOI: 10.1001/jamaoto.2023.3509.

[5] J. Wei, Y. Li, and X. Gui. "Association of hearing loss and risk of depression: a systematic review and meta-analysis". In: *Frontiers in Neurology* 15 (2024), p. 1446262. DOI: 10.3389/fneur.2024.1446262.

[6] Cochlear Americas. *Cochlear Americas Official Website*. https://www.cochlear.com/us/en/home. Abgerufen: 22. September 2025. 2025. URL: https://www.cochlear.com/us/en/home.

[7] M. Kompis, W. Wimmer, and M. Caversaccio. "Long term benefit of bone anchored hearing systems in single sided deafness". In: *Acta Otolaryngologica* 137.4 (Apr. 2017), pp. 398–402. DOI: 10.1080/00016489.2016.1261410.

[8] Ashwin Kumaar Murali Dharan. "A Pilot Study on Developing an Artificial Head for Bone Conduction Devices Testing Purposes". Master's thesis. Gothenburg, Sweden: Department of Electrical Engineering, Chalmers University of Technology, 2021.

[9] W. Kim et al. "Vector of motion measurements in the living cochlea using a 3D OCT vibrometry system". In: *Biomedical Optics Express* 13.4 (Mar. 2022), pp. 2542–2553. DOI: 10.1364/BOE.451537.

[10] Stefan Stenfelt, Bo Håkansson, and Anders Tjellström. "Vibration characteristics of bone conducted sound in vitro". In: *The Journal of the Acoustical Society of America* 107.1 (2000), pp. 422–431. DOI: 10.1121/1.428314.

[11] Anton Husmark and Erik Håkansson. "Estimating Bone Conduction Hearing Perception Using Three-Dimensional Vibration in a Head Simulator: Development and Implementation of a Real-Time Combination Model Enabling Realistic Bone Conduction Hearing Estimation". Master's thesis in Biomedical Engineering. Gothenburg, Sweden: Department of Electrical Engineering, Chalmers University of Technology, 2023.

[12] Douglas Self et al. *Audio Engineering: Know It All*. ISBN-13: 978-1856175265. Newnes (Elsevier), 2008. ISBN: 9781856175265.

[13] Brian C. J. Moore. *An Introduction to the Psychology of Hearing*. Emerald Group Publishing, 1997. ISBN: 0-12-505628-1.

[14] Richard M. Warren. *Auditory Perception*. Cambridge, UK: Cambridge University Press, 1999. ISBN: 0521587832.

[15] Tobias Reichenbach and A. James Hudspeth. "The physics of hearing: fluid mechanics and the active process of the inner ear". In: *Reports on Progress in Physics* 77.7 (2014). Epub 2014 Jul 9, p. 076601. DOI: 10.1088/0034-4885/77/7/076601.

[16] Stefan Stenfelt. "Acoustic and physiologic aspects of bone conduction hearing". In: *Advances in Oto-Rhino-Laryngology*. Vol. 71. 2011, pp. 10–21. DOI: 10.1159/000323574.

[17] S. M. Khanna, J. Tonndorf, and J. E. Queller. "Mechanical parameters of hearing by bone conduction". In: *The Journal of the Acoustical Society of America* 60.1 (1976), pp. 139–154. DOI: 10.1121/1.381081.

[18] R. Dauman. "Bone conduction: an explanation for this phenomenon comprising complex mechanisms". In: *European Annals of Otorhinolaryngology, Head and Neck Diseases* 130.4 (2013), pp. 209–213. DOI: 10.1016/j.anorl.2012.11.002.

[19] Stefan Stenfelt. "Inner ear contribution to bone conduction hearing in the human". In: *Hearing Research* 329 (2015), pp. 41–51. DOI: 10.1016/j.heares.2014.12.003.

[20] Måns Eeg-Olofsson. "Transmission of Bone-Conducted Sound in the Human Skull Based on Vibration and Perceptual Measures". Printed by Kompendiet, Gothenburg. PhD thesis. Gothenburg, Sweden: Institute of Clinical Sciences, Sahlgrenska Academy, University of Gothenburg, 2009. ISBN: 978-91-628-8430-7.

[21] J. Lee et al. "Contralateral bone conducted sound wave propagation on the skull bones in fresh frozen cadaver". In: *Scientific Reports* 13 (2023), p. 7479. DOI: 10.1038/s41598-023-32307-y.

[22] M. Eeg-Olofsson, S. Stenfelt, and G. Granström. "Implications for contralateral bone-conducted transmission as measured by cochlear vibrations". In: *Otol Neurotol* 32.2 (2011), pp. 192–198. DOI: 10.1097/MAO.0b013e3182009f16.

[23] C. Röösli, I. Dobrev, and F. Pfiffner. "Transcranial attenuation in bone conduction stimulation". In: *Hearing Research* 419 (2022), p. 108318. DOI: 10.1016/j.heares.2021.108318.

[24] A. F. Snik et al. "Consensus statements on the BAHA system: where do we stand at present?" In: *The Annals of Otology, Rhinology, and Laryngology. Supplement* 195 (2005), pp. 2–12. DOI: 10.1177/00034894051145201.

[25] J. Liu et al. "Single-sided deafness and unilateral auditory deprivation in children: current challenge of improving sound localization ability". In: *The Journal of International Medical Research* 48.1 (2020), p. 300060519896912. DOI: 10.1177/0300060519896912.

[26] Ruth Y. Litovsky and Matthew J. Goupell. "Introduction to Binaural Hearing". In: *Binaural Hearing*. Ed. by Ruth Y. Litovsky et al. Vol. 73. Springer Handbook of Auditory Research. Springer Nature Switzerland, 2021, pp. 1–15. ISBN: 978-3-030-57099-6. DOI: 10.1007/978-3-030-57100-9_1.

[27] Y. H. An et al. "Long-Term Effects of Hearing Aid Use on Auditory Spectral Discrimination and Temporal Envelope Sensitivity and Speech Perception in Noise". In: *The Journal of International Advanced Otology* 18.1 (2022), pp. 43–50. DOI: 10.5152/iao.2022.21228.

[28] John Clarkson. “Human Capability and Product Design”. In: *Product Experience*. Ed. by Hendrik N.J. Schifferstein and Paul Hekkert. Elsevier, 2008, pp. 165–198. ISBN: 9780080450896. DOI: 10.1016/B978-008045089-6.50009-5.

[29] Lori L. Holt et al., eds. *Speech Perception*. Vol. 74. Springer Handbook of Auditory Research. Springer Nature Switzerland AG, 2022. ISBN: 978-3-030-81541-7. DOI: 10.1007/978-3-030-81542-4.

[30] S. Surendran and S. Stenfelt. “Inter-aural separation during hearing by bilateral bone conduction stimulation”. In: *Hearing Research* 437 (2023), p. 108852. DOI: 10.1016/j.heares.2023.108852.

[31] Renée M. Janssen, Paul Hong, and Neil K. Chadha. “Bilateral Bone-Anchored Hearing Aids for Bilateral Permanent Conductive Hearing Loss: A Systematic Review”. In: *Otolaryngology–Head and Neck Surgery* 147.3 (2012). Reprints and permission: sagepub.com/journalsPermissions.nav, pp. 412–422. DOI: 10.1177/0194599812451569. URL: https://doi.org/10.1177/0194599812451569.

[32] Claudia Priwin et al. “Bilateral Bone-Anchored Hearing Aids (BAHAs): An Audiometric Evaluation”. In: *The Laryngoscope* 114.12 (2004). © 2004 The American Laryngological, Rhinological and Otological Society, Inc., pp. 2131–2134. DOI: 10.1097/00005537-200412000-00019. URL: https://doi.org/10.1097/00005537-200412000-00019.

[33] James O. Pickles. “Auditory pathways: anatomy and physiology”. In: *Handbook of Clinical Neurology*. Ed. by Michael J. Aminoff, François Boller, and Dick F. Swaab. Vol. 129. Elsevier, 2015, pp. 3–25. ISBN: 9780444626301. DOI: 10.1016/B978-0-444-62630-1.00001-9.

[34] Lori L. Holt et al., eds. *Speech Perception*. Vol. 74. Springer Handbook of Auditory Research. Cham: Springer, 2022. ISBN: 978-3-030-81541-7. DOI: 10.1007/978-3-030-81542-4.

[35] Sunil Puria and John J. Rosowski. “Békésy’s contributions to our present understanding of sound conduction to the inner ear”. In: *Hearing Research* 293.1-2 (2012), pp. 21–30. DOI: 10.1016/j.heares.2012.05.004.

[36] Bruno Schratzenstaller et al. “Confirmation of G. von Békésy’s Theory of Paradoxical Wave Propagation along the Cochlear Partition by Means of Bone-Conducted Auditory Brainstem Responses”. In: *ORL* 62.1 (2000), pp. 1–8. DOI: 10.1159/000027707.

[37] N. Kim, K. Homma, and S. Puria. “Inertial bone conduction: symmetric and antisymmetric components”. In: *Journal of the Association for Research in Otolaryngology* 12.3 (2011), pp. 261–279. DOI: 10.1007/s10162-011-0258-3.

[38] M. Zhao, A. Fridberger, and S. Stenfelt. “Vibration direction sensitivity of the cochlea with bone conduction stimulation in guinea pigs”. In: *Scientific Reports* 11.1 (2021), p. 2855. DOI: 10.1038/s41598-021-82268-3.

[39] I. Dobrev and J. H. Sim. “Magnitude and phase of three-dimensional (3D) velocity vector: Application to measurement of cochlear promontory motion during bone conduction sound transmission”. In: *Hearing Research* 364 (2018), pp. 96–103. ISSN: 0378-5955. DOI: 10.1016/j.heares.2018.03.022.

[40] Ivan Dobrev et al. “Sound wave propagation on the human skull surface with bone conduction stimulation”. In: *Hearing Research* 355 (2017), pp. 1–13. DOI: 10.1016/j.heares.2017.07.005.

[41] HBK World / Dytran. *HBK / Dytran Global — Official Website*. https://www.hbkworld.com/web/dytran/global/en. Accessed: 25 September 2025. 2025.

[42] Tobias Neher. "Characterizing the binaural contribution to speech-in-noise reception in elderly hearing-impaired listeners". In: *The Journal of the Acoustical Society of America* 141.2 (2017), EL159. DOI: 10.1121/1.4976327.

[43] Jan Heeren, Giso Grimm, and Volker Hohmann. "The influence of dynamic binaural cues on speech intelligibility in headphone and free-field listening". In: *Fortschritte der Akustik – DAGA 2015*. Universität Oldenburg, Cluster of Excellence Hearing4all. Nürnberg, Germany, 2015, pp. 117–120.

[44] B. Kollmeier et al. "Binaural Hearing in Impaired Listeners: Speech Intelligibility under Spatial Conditions". In: *Audiologische Akustik / Audiological Acoustics* 29.3 (May 1990). ISSN: 0172-8261.

[45] *Swedish Matrix (Hagerman) Test: Instruction Manual for Oldenburg Measurement Applications*. Version 2.2.0.0. Copyright © 2019 HörTech gGmbH. HörTech gGmbH. 2019.

[46] Inga Holube et al. "Einfluss des Maskierers und der Testmethode auf die Sprachverständlichkeit von jüngeren und älteren Normalhörenden". In: *Zeitschrift für Audiologie (Audiological Acoustics)* 48.3 (Jan. 2009), pp. 120–127.

[47] Francis F. Li and Trevor J. Cox. *Digital Signal Processing in Audio and Acoustical Engineering*. 1st. Hardcover; online resource available. Taylor & Francis / CRC Press, 2019, approx. 242. ISBN: 978-1-4665-9388-6.

[48] Vinay K. Ingle and John G. Proakis. *Digital Signal Processing Using MATLAB*. Cengage Learning, 2011. ISBN: 978-1-111-42737-5.

[49] Ahmed A. Shabana. *Theory of Vibration*. Mechanical Engineering Series. Springer Cham, 2019. DOI: 10.1007/978-3-319-94271-1.

[50] M. Geal-Dor, C. Adelman, and H. Sohmer. "Issues Concerning the Mechanisms of Bone Conduction". In: *Audiology Research* 14 (2024), pp. 840–843. DOI: 10.3390/audiolres14050070.

[51] Qian Sun, Wang-Ji Yan, and Wei-Xin Ren. "Analytical Investigation into Error Propagation of Power Spectral Density Transmissibility (PSDT) Based on Coherence Function". In: *Journal of Sound and Vibration* 514 (2021), p. 116429. DOI: 10.1016/j.jsv.2021.116429.

[52] A. W. Phillips and R. J. Allemang. "Frequency Response Function Estimation". In: *Handbook of Experimental Structural Dynamics*. Ed. by R. Allemang and P. Avitabile. The Society for Experimental Mechanics 2020. New York, NY: Springer, 2020, pp. 3–89. DOI: 10.1007/978-1-4939-6503-8_8-1.

[53] P. Dutilleux et al. "Filters and Delays". In: *DAFX: Digital Audio Effects*. Ed. by U. Zölzer. Chichester, UK: John Wiley & Sons, 2011. Chap. 2, pp. 47–81. DOI: 10.1002/9781119991298.ch2.

[54] John Watkinson. *The Art of Digital Audio*. 2nd ed. Oxford, UK: Focal Press, 1994. ISBN: 0-240-51320-7.

[55] Sean Chester et al. "Indexing for Vector Projections". In: *Database Systems for Advanced Applications (DASFAA 2011), Part II, Lecture Notes in Computer Science, vol. 6588*. Ed. by Jeffrey Xu Yu, Myoung Ho Kim, and Rainer Unland. Access provided by 1238 BIBSAM LNCS Sweden. Hong Kong, China: Springer, Berlin, Heidelberg, 2011, pp. 367–376. DOI: 10.1007/978-3-642-20152-3_27.

[56] *Acoustics — Reference zero for the calibration of audiometric equipment. Part 3: Reference equivalent threshold vibratory force levels for pure tones and bone vibrators*. International Organization for Standardization, 2016.

[57] International Organization for Standardization. *ISO389-1:1998 Acoustics — Reference zero for the calibration of audiometric equipment — Part1: Reference equivalent threshold sound pressure levels for pure tones and supra-aural earphones*. ISO Standard, first edition. Published 1998-11-01; withdrawn Dec 13 2017; superseded by ISO389-1:2017. Geneva, Switzerland, Nov. 1998.

[58] Anton Husmark and Erik Håkansson. "Estimating Bone Conduction Hearing Perception Using Three-Dimensional Vibration in a Head Simulator: Development and Implementation of a Real-Time Combination Model Enabling Realistic Bone Conduction Hearing Estimation". Master's thesis. Gothenburg, Sweden: Chalmers University of Technology, 2020.

[59] Stefan Stenfelt and Richard L. Goode. "Bone-Conducted Sound: Physiological and Clinical Aspects". In: *Otology & Neurotology* 26.6 (2005), pp. 1245–1261. DOI: 10.1097/01.mao.0000187236.10842.d5.

[60] Anna Pastusiak et al. "The Benefit of Binaural Hearing Among Listeners with Sensorineural Hearing Loss". In: *Archives of Acoustics* 44.4 (2019), pp. 709–717. DOI: 10.24425/aoa.2019.129726. URL: https://doi.org/10.24425/aoa.2019.129726.

[61] Stefan Stenfelt, Mehrnaz Zeitooni, and Elina Mäki-Torkko. "Evaluating binaural hearing capabilities in individuals with sensorineural hearing loss through bilateral bone conduction stimulation". In: *Scientific Reports* 14.1 (2024), p. 28847. DOI: 10.1038/s41598-024-80379-1. URL: https://doi.org/10.1038/s41598-024-80379-1.

[62] Kirsten Carola Wagener. "Factors Influencing Sentence Intelligibility in Noise". PhD thesis. Oldenburg, Germany: Carl von Ossietzky Universität Oldenburg, 2004. ISBN: 3-8142-0897-8. URL: https://oops.uni-oldenburg.de/460/1/wagfac04.pdf.

[63] Stefan Stenfelt and Mehrnaz Zeitooni. "Binaural hearing ability with mastoid applied bilateral bone conduction stimulation in normal hearing subjects". In: *The Journal of the Acoustical Society of America* 134.1 (2013), pp. 481–493. DOI: 10.1121/1.4807637. URL: https://doi.org/10.1121/1.4807637.

[64] Jan Heeren, Giso Grimm, and Volker Hohmann. "The influence of dynamic binaural cues on speech intelligibility in headphone and free-field listening". In: *To be updated* (2025). Affiliation: Universität Oldenburg, Cluster of Excellence Hearing4all. Contact: j.heeren@uni-oldenburg.de.

[65] Sébastien Santurette and Torsten Dau. "Relating Binaural Pitch Perception to the Individual Listener's Auditory Profile". In: *The Journal of the Acoustical Society of America* 131.4 (2012), pp. 2968–2986. DOI: 10.1121/1.3689554.

[66] Tobias Neher. "Characterizing the binaural contribution to speech-in-noise reception in elderly hearing-impaired listeners". In: *The Journal of the Acoustical Society of America* 141.2 (2017), EL159. DOI: 10.1121/1.4976327. URL: https://doi.org/10.1121/1.4976327.

[67] Birger Kollmeier et al. "The multilingual matrix test: Principles, applications, and comparison across languages: A review". In: *International Journal of Audiology* 54.Suppl 2 (2015), pp. 3–16. DOI: 10.3109/14992027.2015.1020971. URL: https://doi.org/10.3109/14992027.2015.1020971.

[68] Kenneth J. Berry, Janis E. Johnston, and Paul W. Jr. Mielke. *The Measurement of Association: A Permutation Statistical Approach*. Springer Texts in Statistics. Library of Congress Control Number: 2018954500. Mathematics Subject Classifica-

tion (2010): 62Gxx, 62-07, 62-03, 62Axx. Cham, Switzerland: Springer International Publishing, 2019. DOI: 10.1007/978-3-319-98926-6.

A

Appendix 1

A.1 FRF

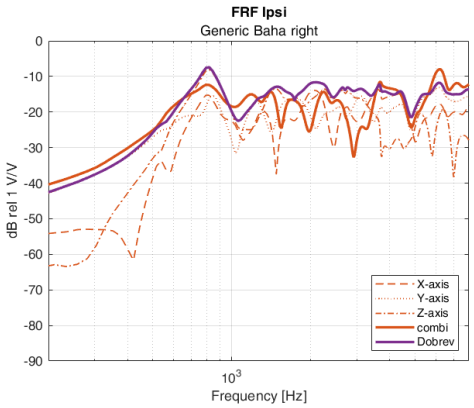

(a) Combined axis

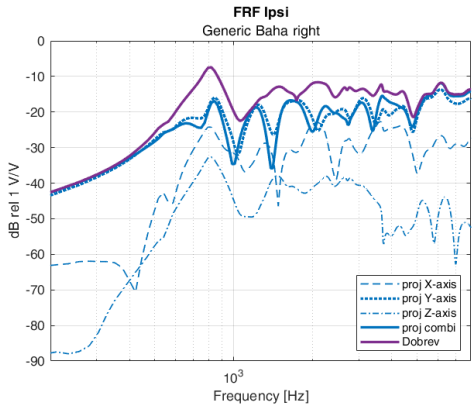

(b) Combined axis with proj. vectors

Figure A.1: Ipsilateral frequency response function.

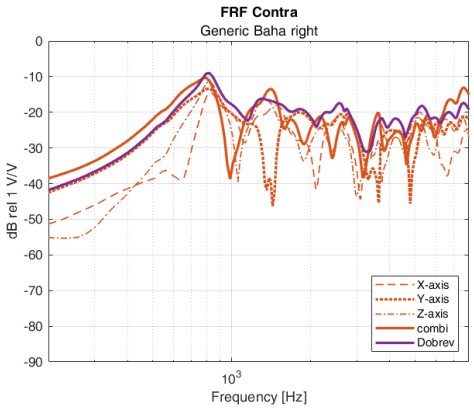

(a) Combined axis

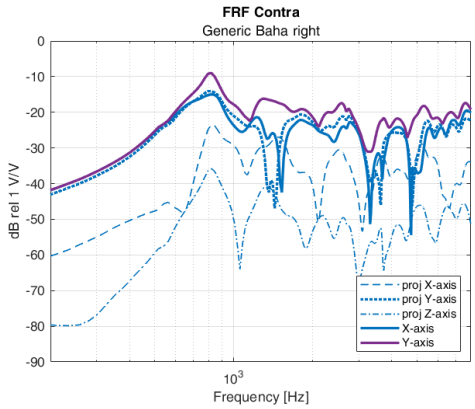

(b) Combined axis with proj. vectors

Figure A.2: Ipsilateral frequency response function.

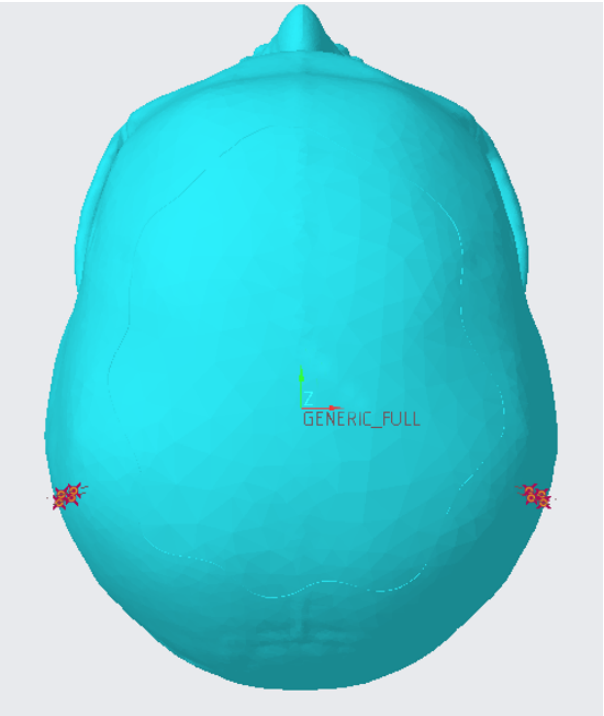

Figure A.3: Top view of the head simulator with read points marking the Baha® position

A.2 Threshold matching

Measure	250	500	750	1000	1500	2000	3000	4000	5000	6000	8000
MAP (dB SPL)	25.5	11.5	–	7	6.5	9	10	9.5	–	15.5	13
RETFL (dB re 1 µN)	-65.5	-72	-73.25	-80.5	–	-85.5	-94	-92	-92.2	-92.5	-92

Table A.1: Transposed Minimal Audible Pressure (MAP) and Reference Equivalent Threshold Sound Pressure Level Values across frequencies according to ISO 389-1 [57].

Axis	Angle from Plane	Component
X_{right}	$\theta_x = 20.8556°$ (from YZ plane)	0.3560
Y_{right}	$\theta_y = 68.8421°$ (from ZX plane)	0.9326
Z_{right}	$\theta_z = 03.4067°$ (from XY plane)	0.0594
X_{left}	$\theta_x = 21.2638°$ (from YZ plane)	0.3627
Y_{left}	$\theta_y = 68.3547°$ (from ZX plane)	0.9295
Z_{left}	$\theta_z = 03.8604°$ (from XY plane)	0.0673

Table A.2: Vector components from plane angles and normalization to a unit vector.

Investigator: Laura Lindel
Supervisor: Jona Hoffmann
29.08.2025

Risk Assessment for Measuring the Speech Reception Threshold on Volunteers, using Head Simulator

The investigation at hand is performed as part of a master thesis at Chalmers University of Technology by Laura Lindel, in collaboration with the Clinical Department at Cochlear Gothenburg Site.

The goal is to enable a realistic simulation of monaural and binaural BAHI fittings under real-life conditions. This thesis thereby lays the groundwork for future product testing under different conditions and with various hearing devices.

Aim of listening experiment:

This investigation aims to measure the Speech Reception Thresholds (SRTs), which is defined as the threshold at which 50% of spoken words are correctly repeated. The data will be compared with findings from clinical studies involving subjects fitted with one and two Bone Conduction Hearing Implants (BAHIs). Due to the limited availability of relevant literature for the head simulator development and the inherent challenges in assessing reliability, this approach has been identified as a suitable method for validating the simulator's performance**.**

Test Setup:

The head simulator is positioned within a loudspeaker array in the test room. The recorded sound is then processed through digital hardware and transmitted directly to the participant's headphones. As a result, the participant—seated in a separate room—experiences the same sound field that the head simulator is exposed to, effectively recreating the auditory scene via headphone playback. The setup is preconfigured and calibrated for normal listening test subject and therefore requires subjectively normal hearing. Individual settings would require the collection of hearing thresholds with is considered sensitive medical information.

The Swedish Matrix (Hagerman) test:

Conducting the Swedish matrix test, is a very common procedure in audiological diagnostics to access speech intelligibility in noise. It measures the Speech Reception Threshold (SRT), the Signal to Noise Ratio at which 50 % of the spoken words are correctly identified by the listener. It consists out of 20 nonsense sentences in a structure as presented in Figure 1. At the beginning of the test the level of the signal and the background noise is the same (65 dB) and as the test continues the level of the signal will automatically be adjusted, based on the answers until the 50 % threshold is reached. The participant selects their response from a list of 50 possible alternatives displayed on a screen (Figure 1) after each sentence is played.

Investigation routine:

First, the participant will state their age and gender. Followingly, the participant will be introduced into the test setup and the test procedure. After all the questions has been answered, the participant starts with a training session, consisting out of a list of 10 words.

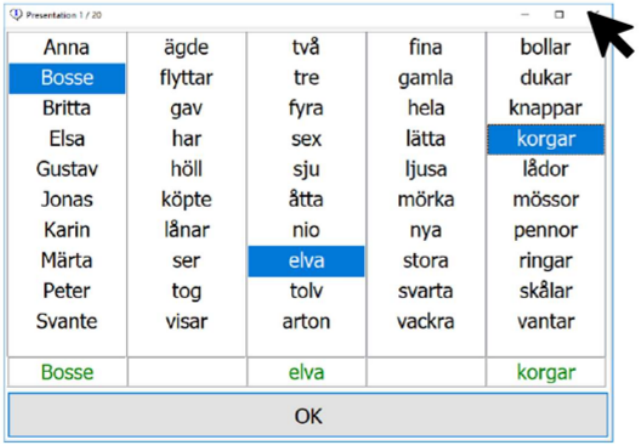

Figure 1 Swedish Matrix (Hagermann) test set.

Test time:

The experiment will include 4 different test conditions, each lasting approximately five minutes. If the test is unable to estimate an SRT it might be necessary to repeat the test round, but not more than one repetitions will be conducted within the session.

Including time for instructions and participant questions, a total duration of around 35 minutes will be expected per participant.

Test group:

For this study, volunteers to participate in the Speech Reception Threshold (SRT) measurements are needed. The data collected from all participants will be used for statistical analysis to identify significant differences across various test conditions. Individual results will not be interpreted or reported separately.

Inclusion criteria

The participant should be a native Swedish speaker with subjectively normal hearing within the age 18 – 65 years.

Exclusion criteria:

Any reports of infection in the head and neck area are exclusion criteria.

Test time:

The experiment will include 4 different test conditions, each lasting approximately five minutes. If the test is unable to estimate an SRT it might be necessary to repeat the test round, but not more than one repetitions will be conducted within the session.

Including time for instructions and participant questions, a total duration of around 35 minutes will be expected per participant.

Test group:

For this study, volunteers to participate in the Speech Reception Threshold (SRT) measurements are needed. The data collected from all participants will be used for statistical analysis to identify significant differences across various test conditions. Individual results will not be interpreted or reported separately.

Inclusion criteria

The participant should be a native Swedish speaker with subjectively normal hearing within the age 18 – 65 years.

Exclusion criteria:

Any reports of infection in the head and neck area are exclusion criteria.

Traceability:
When filling out the booking form, the participants will fill in their name and choose a time slot. In the Case Report Form (CRF) form, the time of the measurement will also be stated. In this way, the investigators can trace the participants if needed, for example in case of a contamination incident. The booking information will be kept save for a duration of 1 month after the last test subject and will be deleted afterward, since complications are expected not to exceed days after the participation of the listening experiment occurring.

General information about In House testing:
- All tests are conducted in accordance with GCP
- The participant can always choose if and when they want to terminate the test, without offering an explanation.

Cochlear	Protocol						
	Subject number						

Baseline visit									
Date:									Time Slot: Start:
	d	d	m	m	y	y	y	y	
									End:

Demographics					
Age (years)	☐ 18-30	☐ 31-40	☐ 41-50	☐ 51-60	☐ 60+
Gender	☐ Female	☐ Male	☐ Other		

Exclusion Criteria	No	Yes
Visible Infection in head/neck area	☐	☐

Inclusion Criteria	Yes	No
I am aware that I always can choose if and when I want to terminate the test, without offering an explanation	☐	☐
I have normal hearing	☐	☐
Native Swedish speaker	☐	☐

Cochlear	Protocol						
	Subject number						

Check	
☐	Cleaning equipment before Experiment
☐	Check Mixer setup **(-27 dB)**
☐	Correct instructions
☐	Fresh batterie (1 per day)
☐	Ventilation off

Results:

Setup		order	SRT	Note:
S0N0 mono	[1]			
S0N90 mono	[2]			
S0N0 stereo	[3]			
S0N90 stereo	[4]			

Comment:

Signature - Laura Lindel	

Cochlear	Protocol						
	Subject number						

Rating:

Please evaluate the amount of **Effort** it took to complete each session

Feel free to use the whole scale, also the space in between the vertical lines.

Round 1

Round 2

Round 3

Round 4

Comment:

DEPARTMENT OF SOME SUBJECT OR TECHNOLOGY
CHALMERS UNIVERSITY OF TECHNOLOGY
Gothenburg, Sweden
www.chalmers.se

CHALMERS
UNIVERSITY OF TECHNOLOGY